https://doi.org/10.5194/egusphere-2022-573
Preprint. Discussion started: 2 August 2022

Importance of size representation and morphology in modelling optical properties of black carbon: comparison between laboratory measurements and model simulations

Baseerat Romshoo[1], Mira Pöhlker[1], Alfred Wiedensohler[1], Sascha Pfeifer[1], Jorge Saturno[2], Andreas Nowak[2], Krzysztof Ciupek[3], Paul Quincey[3], Konstantina Vasilatou[4], Michaela N. Ess[4], Maria Gini[5], Konstantinos Eleftheriadis[5], François Gaie-Levrel[6] and Thomas Müller[1]

[1]Leibniz Institute for Tropospheric Research, 04318, Leipzig, Germany
[2]Physikalisch-Technische Bundesanstalt (PTB), Braunschweig, 38116, Germany
[3]Atmospheric Environmental Science Department, National Physical Laboratory (NPL), Teddington, TW11 0LW, UK
[4]Federal Institute of Metrology METAS, Bern-Wabern, 3003, Switzerland
[5]Environmental Radioactivity Laboratory, Institute of Nuclear & Radiological Sciences and Technology, Energy & Safety (INRASTES), N.C.S.R. Demokritos, Attiki, 15310, Greece
[6]Laboratoire National de Métrologie et d'Essais (LNE), Paris, 75015, France

Correspondence to: Baseerat Romshoo (baseerat@tropos.de)

Abstract

Black carbon (BC) from incomplete combustion of biomass or fossil fuels is the strongest absorbing aerosol component in the atmosphere. Optical properties of BC are essential in climate models for quantification of their impact on radiative forcing. The global climate models, however, consider BC to be spherical particles which causes uncertainties in their optical properties. Based on this, an increasing number of model-based studies provide databases and parametrization schemes for the optical properties of BC using more realistic fractal aggregate morphologies. In this study, the reliability of the different modelling techniques of BC was investigated by comparing them to laboratory measurements. In the first step, the modeling techniques were examined for bare BC particles, and in the second step, for BC particles with organic material. A total of six morphological representations of BC particles were compared, three each for spherical and fractal aggregate morphologies. The BC fractal aggregate is usually modelled using monodispersed particles since their optical simulations are computationally expensive. In such studies, the modelled optical properties showed a 25% uncertainty in using the monodisperse size method. It is shown that using the polydisperse size distribution in combination with fractal aggregate morphology reduces the discrepancy between modelled and measured particle light absorption coefficient σ_{abs} to 10%, for particles with volume mean mobility diameters between 60-160 nm. However, for particles larger than 100 nm, the Absorption Ångström Exponent (AAE) calculated by using a spherical morphology was more consistent with measured value. Furthermore, the sensitivities of the BC optical properties to the various model input parameters such as the real and imaginary parts of the refractive index (m_{re} and m_{im}), the fractal dimension (D_f), and the primary particle radius (a_{pp}) of an aggregate were investigated. The modelled optical properties of BC are well aligned with laboratory-measured values when the following assumptions are used in the fractal aggregate representation: m_{re} between 1.6 to 2; m_{im} between 0.50 to 1; D_f from 1.7 to 1.9, and a_{pp} between 10 to 14 nm. Overall, this study provides experimental support for emphasizing the use of an appropriate size representation (polydisperse size method) and an appropriate morphological representation (aggregate morphology) for optical modelling and parametrization scheme development of BC.

Introduction

Soot particles are produced by incomplete combustion of carbonaceous materials such as fossil fuels, biomass, and biofuels. Black carbon (BC), a major component of soot and also known as light-absorbing carbon, contributes significantly to global warming along with CO2, methane, and volatile organic compounds (VOCs) (IPCC, 2021). On a regional scale, black carbon can significantly perturb the climate (Wang, 2004; Menon et al., 2002). In developing areas such as China, South Asia, and South East Asia, rapid urbanization has caused an alarming increase in the BC mass fraction of the total particle mass concentration (Wiedensohler et al., 2018; Madueno et al., 2019). Moreover, increasing mass concentrations of BC are degrading air quality and causing adverse effects on human health (Pöschl., 2005; Janssen et al., 2011).

High-resolution transmission electron microscopy (TEM) analysis of BC samples from ambient and laboratory studies revealed that BC particles comprise agglomerates made from numerous graphitic soot spherules (Betrancourt et al., 2017; Gini et al., 2016). Over time, BC agglomerates undergo complex changes in their size,

https://doi.org/10.5194/egusphere-2022-573
Preprint. Discussion started: 2 August 2022

morphology, and composition, depending on post-emission atmospheric conditions (Fierce et al., 2015). The BC particles are often found together with other combustion by-products such as organic matter, which enhance the particle light absorption through the lensing effect (Fuller et al., 1999). With increasing residence time of BC in the atmosphere, an aging process occurs, leading to a growth of BC agglomerates into much more compact structures. This is mainly due to the formation of coatings and hygroscopic properties (Petzold et al., 2005; Bond et al., 2006; Abel et al., 2003).

The impact of BC particles on climate is studied by estimating their radiative forcing properties using global climate models (IPCC 2021; Krüger et al., 2022; Jacobson., 2001). In order to simulate the BC radiative forcing in global models, the estimates of various BC optical properties, such as particle light scattering, and mass absorption cross-sections, must be taken into account (Bond et al., 2013; Ciupek et al., 2021). The morphological structure of BC particle plays an important role in determining their light scattering and absorption coefficients (He et al., 2015). The Lorentz-Mie theory (Mie, 1908) is often used to calculate the optical properties of BC particles (Bohren and Huffman, 1983; Bond et al., 2013). This theory is preferred because of the computational simplicity and wide applicability. However, studies have shown large discrepancies in the results of Lorentz-Mie theory when compared with ambient measurements (Adaichi et al., 2010; Wu et al., 2018). Moreover, given the complex aging process of BC agglomerates, it is unrealistic to assume BC particles as spherical particles.

Due to the limitations of the Lorentz-Mie theory, the number of studies on the computation of BC optical properties assuming a fractal morphology has increased (e.g., Berry and Percival, 1986; Kahnert and Kanngießer, 2020; Smith and Grainger, 2014; Liu et al., 2018). To model the optical properties of such fractal BC aggregates, the Rayleigh-Debye-Gans (RDG) approximation (Sorensen, 2011), the discrete dipole approximation DDA (Purcell and Pennypacker, 1973), and the T-matrix method (Mackowski and Mishchenko, 1996) have been used (Adaichi et al., 2010; Kahnert, 2010; Li et al., 2016). Parametrization schemes and databases for the optical properties of BC as fractal aggregates have been developed, and proposed for applications in climate models by Smith and Grainger (2014), Romshoo et al., (2021), Liu et al., (2019), and Luo et al., (2018).

In addition to the various numerical studies conducted on the optical properties of BC aggregates, there is a scientific need to examine the reliability of the modelling techniques, and their comparability with actual measurements. Liu et al., 2018 provided a theoretical overview of how sensitive the radiative properties of soot are to their complex morphologies. The geometric-optics surface wave (GOS) approach was used to calculate the BC light scattering properties at different aging stages and compare them with the measured values (He at el., 2015). Forestierti et al. (2018) measured and modelled the mass absorption cross-sections (MAC_{BC}) for bare flame-generated soot. Due to the high computational time of optical simulations, most of the modelling studies are limited to monodisperse particles (Kahnert, 2010; Adaichi et al., 2010; Kahnert and Kanngießer, 2020; Smith and Grainger, 2014; Romshoo et al., 2021; Liu et al., 2019; Luo et al., 2018). However, for atmospheric applications, ensemble-averaged optical properties for given particle number size distributions are needed (Bond et al., 2013). Therefore, it would be reasonable to investigate the performance of different modelling approaches for calculating the ensemble-averaged optical properties.

The BC aggregate is composed of tiny spherules called "primary particles" or "monomers" (Betrancourt et al., 2017). TEM images show that these primary particles measure between 10 and 30 nm in diameter, depending on the source of combustion, and the interaction among the various mechanisms involved in soot formation (Kholghy et al. 2013; Park et al. 2005). The morphology of the BC aggregates is described by a parameter called fractal dimension D_f (Köylü et al., 1995). Depending on the dynamics of the collisions, and the restructuring and condensation of organic matter present in the atmosphere after emission, the D_f of soot can vary from 1.5 up to ~ 2.8 (Wentzel et al., 2003; Gwaze et al., 2006; Ghazi et al., 2013). The size of the BC primary particle and the fractal dimension are important parameters used in optical modelling studies. However, it is unclear to what extent the assumptions of these input parameters are important when compared to ambient or laboratory measurements.

In this work, we examine modelling methods of BC optical properties for both monodisperse as well as polydisperse aerosol particles. The novelty of this study is the improvement of the modelling techniques for optical properties of BC in order to match their equivalent laboratory measurements. The study is structured as follows. An overview of the laboratory methods is given first, followed by the discussion of the various aspects of modelling the optical properties of BC, such as their representation, selection of the particle sizes, various model input parameters, and the optical model itself. Furthermore, the modelling techniques for two kinds of BC particles are investigated. We begin with modelling the first kind i.e., bare BC particles, evaluating the assumptions of various modelling parameters (for e.g., m_{re}, m_{im}, D_f, and a_{pp}) and comparing them to experimental results. The modelling techniques for the second kind i.e., BC particles with organics is discussed next. Finally, a summary and recommendations for future modelling studies are provided.

2 Methods

2.1 Laboratory generated soot

https://doi.org/10.5194/egusphere-2022-573
Preprint. Discussion started: 2 August 2022

The measurements reported in this study were from two laboratory campaigns for characterization of soot. Experiment E1 involved measurements of thermally denuded nascent soot particles conducted at the National Meteorology Institute of Germany (Physikalisch Technische Bundesanstalt, Braunschweig). In the second experiment (E2), measurements of untreated nascent soot particles were performed at the Leibniz Institute for Tropospheric Research.

2.1.1 Generation of soot particles

For this study, three different miniCAST soot generators (Jing Ltd, Switzerland) were used, which can generate soot particles within a wide range of concentrations, sizes, and chemical compositions (Moore et al. 2014; Ess et al., 2019). Mini-CAST soot generators are diffusion-based or premixed flame-based, which generate soot particles after combustion with a mixture of fuel (propane) and air (Jing et.al, 2014). In the diffusion flame based mini-CAST, propane is mixed with oxidation air at the flame via diffusion, using nitrogen for quenching the flame. In the premixed version of mini-CAST propane and air are mixed before being injected into the flame which results in a premixed (or partially premixed) flame. Depending on the flame type, either of these mini-CASTs can control the soot characteristics by varying the flow rates of fuel, oxidation air, and nitrogen. A key parameter describing the operating conditions of mini-CAST is the overall fuel-to-air ratio, also called the flame equivalence ratio, ϕ. The generator can be operated in a fuel-rich condition when $\phi > 1$, whereas fuel-lean (or near-stoichiometric) condition is defined by $\phi < 1$. Moore et al., 2014 mapped the operation of the soot generator mini-CAST 4202 (Zollikofen BE, Switzerland; Jing 1999) for a wide range of operating conditions, providing an optimal guide for laboratory-based soot generation using a mini-CAST burner. In this study, a total of four mini-CASTs were used with different operating conditions during the both laboratory campaigns. The mini-CASTs were operated at fuel-lean operating conditions with flame equivalence ratios ranging from 0.74 to 1.01, producing soot particles with volume mean mobility diameter ($d_{p,\bar{V}}$) between 53 and 182 nm. Table 1 provides an overview of the operating conditions of the mini-CASTs for both E1 and E2.

Table 1. Details of the different cases in experiments E1 and E2: the operating conditions and resulting properties of the particles such as the mobility diameters ($d_{p,\bar{N}}$ and $d_{p,\bar{V}}$), ratio of the elemental to total carbon (EC/TC), and single scattering albedo (SSA). All the mentioned properties will be defined in the next sections.

Experiment series	Case	Mini-CAST model	Propane (mlpm)	N2/ Mixing air* (lpm)	Oxidation air (lpm)	ϕ	$d_{p,\bar{N}}$	$d_{p,\bar{V}}$	*EC/ TC*	*SSA*
E1	I	MC 5203C	140	0.61	3.30	1.01	38	60	-	0.014
E1	II	MC 5203C	140	0.56	3.60	0.93	71	106	-	0.024
E1	III	MC 5203C	140	0.33	3.30	1.01	105	160	-	0.074
E1	IV	MC 5203C	84	0.00	2.72	0.74	105	160	-	0.042
E2	V	MC 5201BC	60	0.42	1.10	0.94	56	83	0.35	0.011
E2	VI	MC 5201BC	60	0.39	1.10	0.96	89	126	0.69	0.053
E2	VII	MC 5201BC	60	0.23	1.30	0.94	129	181	0.68	0.062
E2	VIII	MC 5203C	140	0.56	3.60	0.93	48	86	0.35	0.054
E2	IX	MC 5203C	140	0.00	3.30	1.01	122	174	0.66	0.112
E2	X	MC 5303C	140	0.30	4.20	0.80	84	122	0.68	0.045
E2	XI	MC 5303C	140	0.00	4.20	0.80	122	181	0.62	0.083

*For mini-CAST 5201BC

2.1.2 Objectives of laboratory experiment E1 and E2

Experiment E1: The objective this experiment was to obtain the size, and the optical properties of soot particles after removal of the volatile organic content, which are expected to represent bare black carbon particles as closely as possible. Figure A1 shows a schematic of the experimental setup used in experiment E1. The soot particles were produced with a mini-CAST 5203 Type C. The mini-CAST 5203C consists of three diffusion flames, generating soot particles under fuel-lean operating conditions. The aerosols generated from mini-CAST 5203C were passed through a Catalytic Stripper (Catalytic Stripper Model CS015, Catalytic Instruments, Rosenheim, Germany) to remove the volatile contents, in this case, mainly organic carbon. For each case in E1 (Table. 1), the Catalytic Stripper was operated at unheated condition, at 150°C condition (BC particles pass through the Catalytic Stripper operated at 150°C), and at 350°C condition (BC particles pass through the Catalytic Stripper at 350°C). Particles coming out of the Catalytic Stripper are then passed through several instruments that measure particle

https://doi.org/10.5194/egusphere-2022-573
Preprint. Discussion started: 2 August 2022

number size distribution, particle light extinction, absorption, and scattering. Detailed information about these measurements is provided in Appendix A.

Experiment E2: In this experiment, the size, the composition, and the optical properties of untreated nascent soot particles produced by the different mini-CAST burners at different operating conditions were measured. The schematic diagram of the experimental setup used in E2 is shown in Figure A2. Three mini-CAST models were used in this experiment including a mini-CAST 5203 Type C, a mini-CAST 5201 Type BC, and a mini-CAST 5303 Type C were used. The mini-CAST 5201BC burner was operated in the partially premixed flame mode (Ess et al. 2019, Ess et al. 2021). The flow settings of propane, nitrogen or mixing air (mini-CAST 5201 BC), and oxidation air were adjusted in order to obtain soot particles of specific size, as shown in Table 1 by the corresponding number mean mobility diameter ($d_{p,\bar{N}}$), and the volume mean mobility diameter ($d_{p,\bar{V}}$). The details of the flow settings for the three mini-CAST models used are shown in Table 1. The particles generated from the soot generators are delivered to various instruments to measure their number size distributions, aerosol mass concentration, chemical composition, particle light extinction, absorption, and scattering coefficients. The details about the instrumentation used are shown in Appendix A.

2.2 Fundamentals of modelling optical properties of soot particles

2.2.1 Morphology of soot and representations for modelling

In order to model the optical properties of soot, it is important to choose the most appropriate morphological representation for soot particle. This step is considered particularly important because the modelled optical properties were further validated with the measurements from E1 and E2. TEM images were not available for this study, therefore, the morphological representations of soot were selected based on TEM images from a previous laboratory study using the mini-CAST generators (Ess et al., 2021). In addition to the TEM images from Ess et al. (2021), the operating conditions of the mini-CAST burners during experiments E1 and E2 (Table. 1), and the fraction of organic carbon of soot particles from E2 were also kept in mind while selecting the morphological representations.

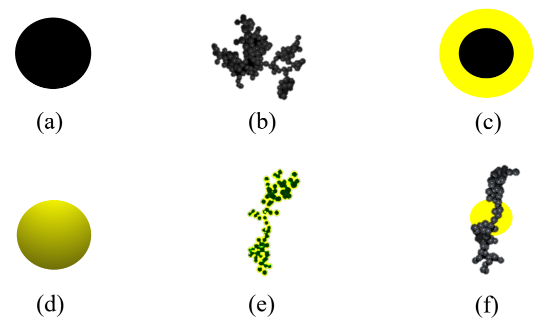

Figure 1. Morphological representations of soot used in this study: **(a) sphere, (b) aggregate, (c) coated sphere, (d) homogeneously mixed sphere, (e) coated aggregate , and (f) aggregate partly enclosed in sphere.**

For modelling the particles from the denuding experiment E1, the simulated particles are assumed to be bare black carbon, since a Catalytic Stripper was used to remove the volatile organic matter. However, the Catalytic Strippers was not able to remove the entire organic matter, leaving some residuals behind. This must be noted when comparing the modelled optical results with their equivalent laboratory measurements.

Two morphological representations of bare BC particles were used as shown in Figure 1(a, b). The first one is a sphere(Fig. 1a); the second one is a fractal aggregate(Fig. 1b). The "sphere" representation is the most simplified representation used by fellow researchers (Bond et al., 2013). An "aggregate" representation shows the realistic morphology of the BC aerosols when they are formed by combustion (Michelsen et al., 2017; Ess et al., 2021). The morphology of such fractal aggregates is mathematically described by Eggersdorfer et al., (2011):

$$N_{\mathrm{pp}} = k_{\mathrm{fm}} \left(\frac{D_{\mathrm{p}}}{2a_{\mathrm{pp}}}\right)^{D_{\mathrm{fm}}}, \qquad (1)$$

https://doi.org/10.5194/egusphere-2022-573
Preprint. Discussion started: 2 August 2022

where, a_{pp} is the radius of primary particles, N_{pp} is the number of primary particles, D_{fm} is the mass-mobility exponent, D_p is the mobility diameter, and k_f is a dimensionless pre-factor.

In the experiment E2, additional information about the chemical composition of the soot particles were available from the EC/OC analysis conducted on the loaded quartz filters. Based on the EC/OC analysis results, the various morphological representations of BC particles with organics are simulated. Four models for BC particles with organics were used to represent the particles generated from E2. The four representations are shown in Figure 1 (c) to (f) for coated spheres, homogeneously mixed spheres, coated aggregates and aggregates partly enclosed in sphere. The "coated sphere" comprised of an inner spherical BC core enclosed within a shell of organic carbon. In the "homogeneously mixed sphere", BC and organic carbon were internally mixed following the volume mixing rule (Chylek et al., 2000) to form a homogenized mixture. The "coated sphere" and "homogeneously mixed sphere" are the simplified models to represent coated BC aerosols. The "coated aggregate" is a realistic representation, morphologically similar to the "aggregate" (Figure 1b), with the difference that each monomer is coated with a layer of organic carbon. Finally, the "aggregates partly enclosed in sphere" represented a model for aged soot, comprising of an "aggregate" (Figure 1b) immersed in a sphere of organic carbon. Since this study simulates laboratory-produced soot, the particles are not likely to resemble those in the "aggregates partly enclosed in sphere" representation. It was nevertheless included in the study for the sake of comparison. Further details of how the six morphological representations shown in Fig. 1 were modelled will be explained in the following sections.

2.2.2 Construction rules for spherical particles

In the "sphere" and "homogeneously mixed sphere" representation, the diameters of the spheres were taken from the SMPS size distributions obtained from the laboratory experiments. The "coated sphere" representation consisted of two spheres; the diameter of the outer sphere (D_o) was directly taken from the SMPS size distributions. The diameter of the inner sphere (D_i) was obtained by:

$$D_i^3 = (1 - f_{oc})\, D_o^3, \tag{2}$$

where f_{OC} is the fraction of organic carbon obtained from the results of EC/OC analysis as:

$$f_{oc} = 1 - \frac{EC}{TC} = 1 - \frac{EC}{EC+OC} \tag{3}$$

where $\frac{EC}{TC}$ is the volume ratio of elemental carbon to the total carbon ($TC = OC + EC$). The volume ratio is derived from the EC/OC analysis after dividing the masses by their respective densities. In this study, it was assumed that elemental carbon corresponds to black carbon. The density of elemental carbon ρ_{EC} was taken as 1.8 g cm^{-3} (Park et al., 2004), and the density of organic carbon as 1.1 g cm^{-3} (Schkolnik et al., 2007).

2.2.3 Construction rules for aggregate particles

For simulating the "aggregate", "coated aggregate", and "aggregate and sphere" representations, the number of primary particles N_{pp} per aggregate, and the radius of primary particle a_{pp} must be determined. In previous studies comparing modelled and measured optical properties of soot aggregates, the N_{pp} was determined by dividing the measured mass of total particle by the estimated mass of a spherule (Forestierti et al., 2018); or reconstructed using results from TEM analysis (He et al., 2015). In our study, we investigated the methods for estimating the N_{pp} in absence of mass or TEM results. Three different conversion methods for calculating the number of primary particles N_{pp} per aggregate were applied in this study. In the first method by Rissler et al. 2012, the aggregate mass is divided by the mass of a single primary to obtain N_{pp}. The second technique described by Sorensen. (2011) uses the mobility mass scaling exponent in conjunction with the concept that black carbon aggregates fall into the slip regime. The third method, developed by Schmidt-Ott. (1988) is based on a power law function. Further details of the three methods are provided in Appendix B.

The radius of primary particle a_{pp} is used in all the three methods for calculating the number of primary particles N_{pp} per aggregate. Diffusion flame-based generators like the mini-CAST burners, produce soot primary particle radius (app) between 4 and 14 nm (Bourrous et al., 2018; Mamakos et al., 2013). Due to absence of measurements of a_{pp}, and for the sake of simplicity, a constant value a_{pp} = 14 nm was used for the entire study, except for the part of sensitivity analysis discussed in the next section.

In the "coated aggregate" representation, a layer of organic carbon was present around each primary particle comprising the soot aggregate. The thickness of this layer of organic carbon is the difference between the outer radius of the primary particle (a_o), and the inner radius of the primary particle (a_{in}). Following equation (2), the

https://doi.org/10.5194/egusphere-2022-573
Preprint. Discussion started: 2 August 2022

relationship between the fraction of organic carbon (f_{oc}), the outer radius of the primary particle (a_o) and the inner radius of the primary particle (a_{in}) were determined. It must be noted that in the "coated aggregate" representation, the size of the primary particles in the aggregates generated from the Diffusion Limited Aggregation (DLA) software is equal to the outer radius of the primary particle (a_o). In the next step, a smaller sphere with the inner radius of the primary particle (a_{in}) was placed inside each primary particle.

In the "aggregate partly enclosed in sphere" representation, after generating an aggregate comprising of black carbon, a sphere of organic carbon was placed at the center of mass of the black carbon aggregate. The radius of the sphere of organic carbon (R_{so}) is obtained by:

$$R_{so}{}^3 = f_{oc}(a_{app}{}^3 \cdot N_{pp}), \quad (4)$$

When a sphere of organic carbon is placed around parts of BC aggregate in the"aggregate partly enclosed in sphere" representation, the parts of black carbon aggregate inside the sphere reduces the volume of organic carbon. Iteratively increasing the radius of the sphere of organic carbon would replace this lost volume. In this study, since non-compact aggregates were used and the amount of organic coating was less than 70%, only a small portion of BC aggregate was present inside the organic sphere. A sensitivity study was conducted to test how the absorption cross-section changes when the radius of the sphere of organic carbon is iteratively increased. The results of this sensitivity analysis showed that the absorption cross-section varied by 2 to 3% after iteratively increasing the radius of the organic carbon sphere. Thus, for the sake of simplicity, the particles were left as they are. However, when modelling coated aggregates with more compact structures or high coating fractions, it is recommended to apply the iteration schemes to each particle.

2.2.4 Other parameters from literature

Simulation of optical quantities with scattering calculations requires a number of assumptions about the morphology of the particles and the refractive indices. This section explains the assumptions and their implementation in the scattering model.

In the first experiment, E1, the composition of the simulated morphological representations "sphere", and "aggregate" was assumed to be bare black carbon, i.e., elemental carbon in nature. The real and imaginary parts of the refractive index, m_{re} and m_{im}, respectively, were taken from a study by Kim et al., 2015. The values of m_{re} and m_{im} for EC at wavelengths of 467, 530, and 660 nm are summarized in Table A2. The refractive index of the OC in experiment E2 is also taken from Kim et al., 2015, for the representations of "coated sphere", "coated aggregate", and "aggregate partially enclosed in sphere". However, for the "homogeneously mixed sphere", the effective complex refractive index m was calculated from the volume-mixing rule (Chylek et al., 2000). The values of m_{re} and m_{im} for OC used in this study are summarized in Table A2.

In the "aggregate", "coated aggregate", and "aggregate partially enclosed in sphere" representation, the morphology of the particle is described by the fractal dimension D_f. The representative values for D_f for freshly emitted soot particles near the combustion source ranges from 1.6 to 1.9 (Gwaze et al., 2006). Transmission electron microscopy (TEM) analysis of soot samples from different engines showed values for the fractal dimensions between 1.5 and 2.1 for diesel soot and 2.2 and 3.0 for spark-ignition engines (Wentzel et al., 2003). In this study, the value of D_f in all the aggregate representations was set to 1.7, except for the sensitivity analysis. The D_f of 1.7 is commonly representative of laboratory-generated fresh soot and was used after examining the TEM images from the mini-CAST generator provided in Ess et al. (2021).

A sensitivity analysis of various modelling parameters, like the refractive index, fractal dimension, and radius of the primary particle were conducted in this study to understand their relative importance towards the modelled optical properties. The results of the sensitivity study were focused on the bare particles from denuding experiment E1, excluding the impact of an organic coating. For studying the sensitivity of a_{pp}, the optical properties were modelled for a_{pp} ranging from 5 to 25 nm. In the sensitivity study of D_f, the optical properties are compared and validated for the "aggregate" representation for D_f ranging from 1.5 - 2.8. The dependency of the modelled optical properties on the real and imaginary parts of refractive index was also studied. The optical properties were modeled using "aggregate" and "sphere" representations for the real part of the refractive index m_{re} ranging from 1.2 to 2, and the imaginary part of the refractive index m_{im} ranging from 0.2 to 1. For all the results of the sensitivity study, the modelled optical properties were compared with their laboratory equivalents for an better understanding of the subject.

2.3 Tools for modelling soot optical properties

Aggregation of soot agglomerates to form a larger soot fractal aggregate is described by the process of diffusion-limited cluster aggregation (Witten and Sander, 1983). Based on this principle, various Diffusion-limited algorithms (DLAs) have been developed. The tunable diffusion limited aggregation (DLA) software (Woźniak,

https://doi.org/10.5194/egusphere-2022-573
Preprint. Discussion started: 2 August 2022

2012) was used in this study to simulate the "aggregate", "coated aggregate", and "aggregate and sphere" soot representations. This algorithm preserves fractal characteristic of the aggregate, by iteratively adding each primary particle one by one.

The Multi-Sphere T-matrix Method (MSTM) code (Mackowski et al., 2013) and the Lorentz-Mie theory (Hergert and Wriedt, 2012; Bohren and Huffman, 1983) were used to model the optical properties of simulated soot particles. The optical properties were calculated in the visible spectrum, for λ equal to 467, 530, and 660 nm. It must be noted that the range of λ was limited as only refractive index at the wavelengths 467, 530, and 660 nm were available (Kim et al., 2015).

For the "sphere", the "homogeneously mixed sphere" and the "coated sphere" representations, the Python Mie Scattering package PyMieScatt (Sumlin et al., 2018) based on the Lorentz-Mie theory was used. The MSTM code was used for the "aggregate", "coated aggregate", and "aggregate and sphere" representations. The MSTM code contains a FORTRAN based algorithm that calculates the optical properties of a set of arbitrary spheres (Mackowski and Mishchenko, 2011; Mishchenko et al., 2004). The MSTM code is therefore appropriate for computing the radiative properties of aggregates. The MSTM code has found wider applications in the research field because of better accuracy and comparatively lower computational cost for fractal like particle compared to other methods like the Discrete Dipole Approximation DDA (Liu et al., 2017).

The MSTM manual notes a limitation that the nested spheres in the particle should not intersect each other. However, in the case of "aggregate and sphere" representation (Fig. 1f) the monomers of the aggregate intersected with the sphere at few points. The application of the MSTM code over particles with few intersecting spheres were tested by comparing them to the results of the Geometric Optics Surface-wave (GOS) approach used in the study by He et al. (2015). The results for the absorption cross section from both the methods were in good agreement with each other, summarized in the supplementary information of this manuscript. Therefore, the MSTM code was used for the case of "aggregate and sphere" representation where few intersecting spheres were present.

The MSTM code and the Lorenz-Mie theory were used to calculate the extinction efficiency Q_{ext}, absorption efficiency Q_{abs}, scattering efficiency Q_{sca}, and the asymmetry parameter g. The asymmetry parameter g is defined as the intensity-weighted average of the cosine of the scattering angle. The single scattering albedo (SSA) was further derived from the ratio of the scattering efficiency (Q_{sca}) to the extinction efficiency (Q_{ext}) as:

$$\mathrm{SSA} = \frac{\sigma_{sca}}{\sigma_{ext}}. \tag{5}$$

The mass absorption cross section of black carbon (MAC_{BC}) is calculated from the ratio of absorption cross section (C_{abs}) and BC mass (m_{BC}) as:

$$MAC_{BC} = \frac{C_{abs}}{m_{BC}}, \tag{6}$$

where ρ_{BC} is the density of black carbon and taken in this study to be 1.8 g cm^{-3} (Park et al., 2004).

The absorption Ångström exponent AAE describes the wavelength dependence of the aerosol light absorption. The AAE was calculated from the best fit of $\sigma_{abs}(\lambda)$ at the wavelengths λ of 470, 520, and 660 nm by:

$$\sigma_{abs}(\lambda = 467, 530, 660\ nm) = C_o \lambda^{-AAE}, \tag{7}$$

where C_o is a constant. It must be noted that the use of wavelengths λ of 467, 530, and 660 nm for calculations is a result of the availability of the refractive indices nm (Kim et al., 2015) at which the modelled optical properties are calculated.

The absorption coefficient σ_{abs} (unit: Mm^{-1}) is the sum of the absorption cross-section C_{abs_i} (unit: m^2) calculated for each available size range:

$$\sigma_{abs} = \sum_{d_i=1}^{d_n} C_{abs}(d_i) \cdot n(d_i), \tag{8}$$

where n is the number concentration of the size range with diameter d_i. The absorption cross-section C_{abs} is calculated from the absorption efficiency Q_{abs} for each size range as:

$$C_{abs}(d_i) = Q_{abs}(d_i) \cdot \pi \frac{{d_i}^2}{4} \cdot, \tag{9}$$

Similarly, the scattering coefficient σ_{sca} and the extinction coefficient σ_{ext} are derived.

https://doi.org/10.5194/egusphere-2022-573
Preprint. Discussion started: 2 August 2022

2.3.1 Size of the simulated soot particles

The optical properties were modelled for monodisperse and polydisperse number size distributions. The definitions for both the size distribution methods are given below:

- Monodisperse size distribution method: the optical properties were modelled for a single particle whose size was the mean diameter $d_{p,\bar{N}}$ of the number size distribution or the volume mean diameter $d_{p,\bar{V}}$ derived from the volume size distribution. The monodisperse size distribution method is commonly used in modelling studies of BC where the results are usually focused on single sized particles (e.g., Berry and Percival, 1986; Kahnert and Kanngießer, 2020; Smith and Grainger, 2014; Liu et al., 2018; Liu et al., 2019; Luo et al., 2018).

- Polydisperse size distribution method: the modelled optical properties are integrated over size according to the particle number size distribution. This ensemble-averaged size method is more relevant to ambient or laboratory studies of BC, where the optical properties are measured for a broad size distribution.

From this point forward, monodisperse and polydisperse size distribution methods will be referred to simply as "monodisperse method and "polydisperse method", respectively. Figure 2 provides an overview of Sec. 2, including the various experimental cases, morphological representations, and size distribution methods used to model the optical properties.

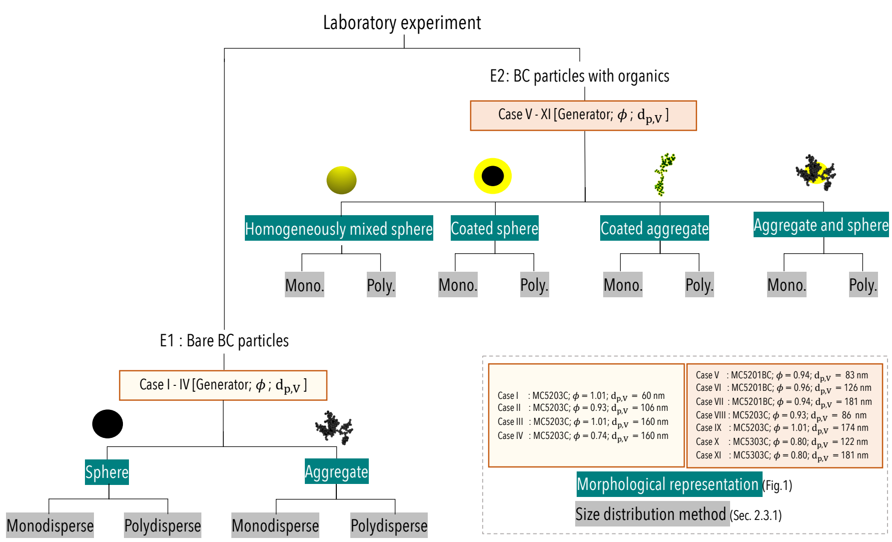

Figure 2. Schematic overview of the various experimental cases, morphological representations, and size distribution methods used to model the optical properties.

3 Results

3.1 Denuding experiment E1 - modelling techniques for bare BC

The Single Scattering Albedo (SSA), and the Absorption Ångström Exponent (AAE) measured from the three heating conditions of the denuding experiment E_1 are shown in Fig. 3. In cases *I-III*, as the particles were heated to remove the organic matter, the SSA and AAE values decreased. On the other hand, in case *IV* where ϕ is 0.74 and particles contain a lower amount of organic matter (Mamakos et al., 2013), both SSA and AAE are not significantly decreased by heating. This section is about modelling the optical properties of bare BC. Therefore, only the experiments with the catalytic stripper at 350 °C are used, since in this case the soot has the comparatively lowest organic carbon content.

https://doi.org/10.5194/egusphere-2022-573
Preprint. Discussion started: 2 August 2022

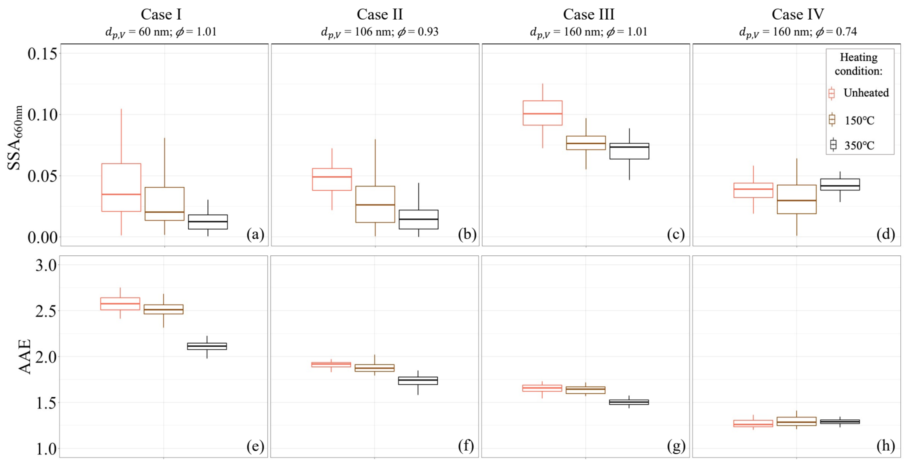

Figure 3. Measured optical properties for the four cases of experiment E1. Panels **(a-d)** show single scattering albedo (SSA), and **(e-h)** show Absorption Ångström Exponent (AAE). In each panel, the box-plots are arranged for three heating conditions where the BC particles bypass the Catalytic Stripper (unheated) or pass through the Catalytic Stripper operated at 150°C or 350°C, respectively. The operating condition is indicated in the legend on the top-right of the figure.

3.1.1 Comparison of optical properties of monodisperse bare aggregates with different methods of calculating the primary particle number

The three methods for estimating the number of primary particles (N_{pp}) were compared using both $d_{p,\bar{N}}$ and $d_{p,\bar{V}}$ for the four cases of E1. The results of this section are relevant for the morphological representations consisting of a fractal aggregate such as "aggregate", "coated aggregate", and "aggregate and sphere". The BC fractal aggregates were simulated using the N_{pp} calculated from the three methods, and the SSA was modelled, as shown in Fig. 4. In order to compare the modelled results with the experimental values, the measured SSA is also shown in Fig. 4. When calculating the N_{pp} using $d_{p,\bar{N}}$, the results of modelled SSA showed variability of up to a factor of 2 with respect to the three methods. In contrary, when $d_{p,\bar{V}}$ is used for calculation of N_{pp}, the difference in the results of modelled SSA changed up to a factor of 2.8. It was not possible to recommend one method due to the differences in results from the three methods depending on the size. However, since the method by Sorensen (2011) involved the least amount of assumptions, it was used as a standard method in this manuscript.

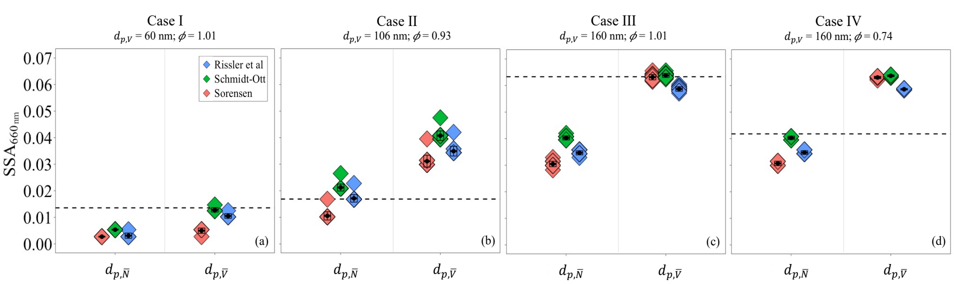

Figure 4. Modelled single scattering albedo (SSA) of bare BC aggregates using the three methods for calculation of the primary particle number (Rissler et al., 2013; Sorensen, 2011; and Schmidt-Ott, 1988). Panels **(a-d)** show the results for the four cases of E1. For each case, the three methods were applied to calculate the N_{pp} using both the $d_{p,\bar{N}}$ and $d_{p,\bar{V}}$ (x-axis). The mean of the modelled *SSA* for each method is shown by the black point. The dashed line in the panels represents the mean of the experimentally measured *SSA*.

3.1.2 Optical properties of spherical and fractal bare BC particles using the monodisperse method

The single scattering albedo (SSA) and absorption ångström exponent (AAE) of bare BC particles generated in experiment E1 were modelled using the monodisperse method and compared the experimentally measured values. Fig. 5(a-d) shows the modelled SSA for the cases I - IV of E1 using the "sphere" and "aggregate" representation. For each of the representation, the SSA was modelled using both $d_{p,\bar{N}}$ and $d_{p,\bar{V}}$. In general, it was observed that "sphere" representation had a higher SSA. Previous studies have also noted an increase in scattering as the particles becomes more compact in shape (Luo et al., 2018; Smith and Grainger, 2014; Li et al., 2016). Moreover, when compared to measured values, in the cases II – IV (Fig. 5b-d), the modelled SSA was overestimated when using the "sphere" representation by up to a factor of 2 to 5. Only in the case *I,* with $d_{p,\bar{V}}$ = 60 nm, the modelled SSA using the "sphere" representation fell in the range of measured values. As the BC particle increases in size, from case I to IV, there was an increase in the overestimation from the results of "sphere" representation. When using the "aggregate" representation, the modelled SSA results fall in line with or are close to the measured SSA. Therefore, modelling the SSA using "aggregate" representation reproduced results closely matching the measured values.

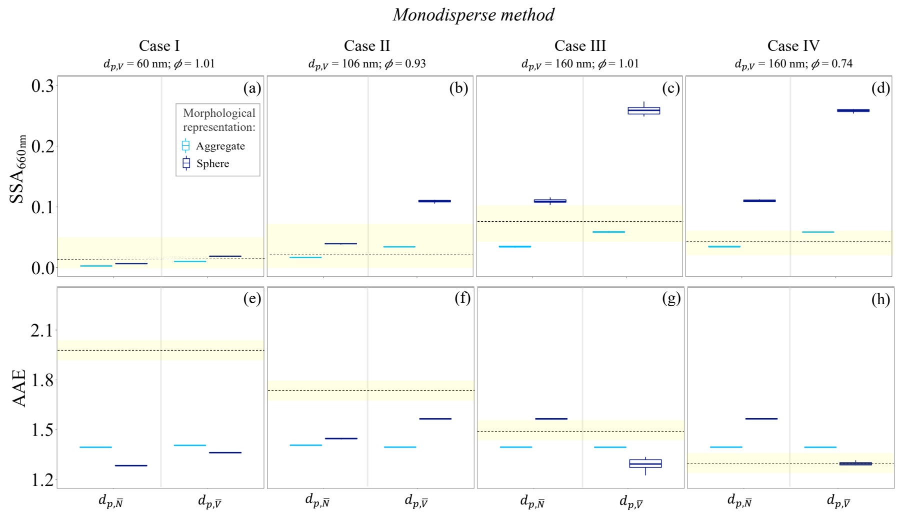

Figure 5. Optical properties of bare BC particles modelled using the monodisperse method compared to their measured values. Panels **(a-d)** show single scattering albedo (SSA), and **(e-h)** show absorption ångström exponent (AAE) for the cases I – IV of E1. In each panel/case, the "sphere" and "aggregate" representation for bare BC particles was used as shown in the legend. The SSA and AAE is modelled using both $d_{p,\bar{N}}$ and $d_{p,\bar{V}}$ (X-axis). The shaded yellow area represents the experimentally measured values, with the dashed line being the mean of the measured SSA or AAE. The lower hinge and the upper hinge of the boxplot represent the 25% and 75% quantile of the observations, respectively. The lower whisker is equal to the smallest observation greater than or equal to lower hinge - 1.5*IQR. Similarly, the upper whisker is equal to the largest observation less than or equal to upper hinge + 1.5*IQR. The meaning of these terms is consistent for boxplots through this study.

Figure 5(e-h) shows the AAE for the E1 cases (I - IV) modelled using the monodisperse method. For smaller particles ($d_{p,\bar{V}}$ = 60, 106 nm), the measured AAE was larger than the modelled AAE by a factor of up to 1.6. In contrast, the measured and modelled AAE agreed better for larger particles ($d_{p,\bar{V}}$ = 160 nm). Smaller particles contain a greater amount of organic carbon than larger particles (Zhang et al., 2020), which makes removing all organic carbon difficult with Catalytic Stripper. This results in a higher measured *AAE* ~1.75 and ~2.1 in smaller particles with $d_{p,\bar{V}}$ of 60 and 106 nm (Liu et al., 2018). This information must be taken into account when modeling smaller denuded particles as bare BC particles. Liu et al. (2018) found that the modelled *AAE* for bare BC particles was higher in the case of aggregate morphology than when a spherical structure was assumed. In this study, the results of the aggregate and spherical morphology were dependent on the size of the particles. Overall, for larger particles ($d_{p,\bar{V}}$ = 160 nm), the modelled AAE from the "sphere" representation was in better agreement when compared to measured values.

https://doi.org/10.5194/egusphere-2022-573
Preprint. Discussion started: 2 August 2022

3.1.3 Optical properties of spherical and fractal bare BC particles using the polydisperse method

The optical properties of bare BC particles were modelled using the polydisperse size method and compared the experimentally measured values. Figure 6(a-d) compares the modelled SSA with the measured SSA at a wavelength of 660 nm. As observed in the previous results of SSA modelled using the monodisperse method (Fig. 5), in this case also the modelled SSA match closely to the measured SSA when using the "aggregate" representation. Additionally, the modelled SSA was compared with the measured values for three wavelengths in the visible range shown in Fig. S2. The trends were uniform for all the three wavelengths following the results in Fig. 6(a-d).

Similarly, the modelled σ_{abs} using polydisperse method is compared with the measured $\sigma_{abs}{}^{AE33}$ in Fig. 6(e-h). The modelled σ_{abs} using the "aggregate" representation was in excellent agreement with the measured $\sigma_{abs}{}^{AE33}$. Whereas, the σ_{abs} modelled using the "sphere" representation overestimated the BC particle absorption, especially in larger particles (case III and IV). He at al. (2014) found that the absorption modelled for single-sized BC particles was underestimated by up to 25%, when compared to measured values. In this study it was demonstrated that this discrepancy between modelled and measured absorption results can be reduced to 10%, when using the polydisperse method, in combination with an "aggregate" representation of soot. The modelled σ_{abs} was compared with the measured $\sigma_{abs}{}^{AE33}$ for three wavelengths in the visible range shown in Fig. S2. The results in Fig. S2 were in agreement with those found in Fig. 6(e-h).

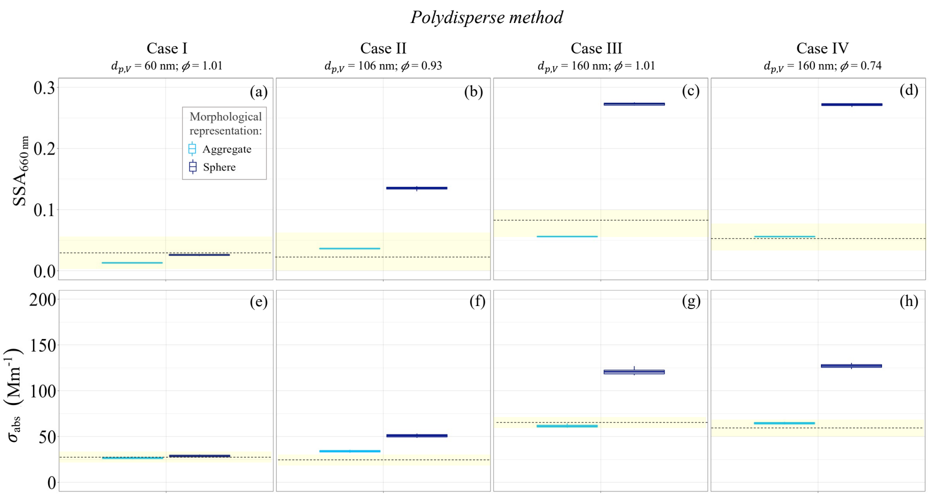

Figure 6. Optical properties of bare BC particles modelled using the polydisperse method compared to their measured values. Panels **(a-d)** show single scattering albedo (SSA), and **(e-h)** show absorption coefficient (σ_{abs}) for the cases I – IV of E1. In each panel/case, the "sphere" and "aggregate" representation for bare BC particles was used as shown in the legend. The shaded yellow area represents the experimentally measured values, with the dashed line being the mean of the measured SSA or σ_{abs}.

3.1 Modelling techniques for bare BC – sensitivity study

3.2.1 Refractive index

The optical properties of bare BC particles were studied as a function of the real part of the refractive index m_{re}. Figure 7(a) shows the results of SSA with m_{re} varying from 1.2 – 2, for the case III ($d_{p,\bar{V}}$ = 160 nm) of E1. In case of the "sphere" representation, the SSA was highly sensitive to the m_{re}, increasing by a factor of up to 2.5. Comparatively, the SSA calculated from the "aggregate" representation was less sensitive to the m_{im}. It can be seen that the modelled SSA using the "aggregate" representation is in good agreement with the measured results when m_{re} is between 1.6 - 2. Similarly, the modelled AAE with respect to the m_{re} for the "sphere" and "aggregate" representation is shown in Fig. 7(c). Similar to the results shown in Fig. 7(a), the AAE modelled by "sphere" representation is highly sensitive to the m_{re}. It was inferred that the modelled values closely match the measured AAE when m_{re} is taken between 1.6 – 2. Overall, the optical properties of spherical particles had a higher sensitivity to the m_{re} than the aggregate particles.

https://doi.org/10.5194/egusphere-2022-573
Preprint. Discussion started: 2 August 2022

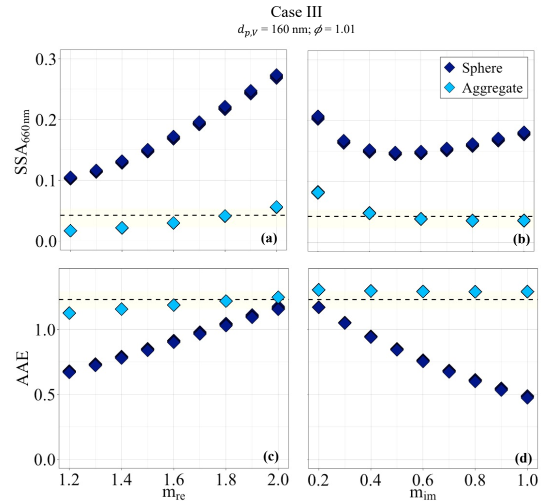

Figure 7. Optical properties of bare BC particles studied as a function of real part and imaginary part of the refractive index (m_{re} and m_{im}) . The results are shown for *SSA* **(a and b)** and AAE **(c and d)** for the case *III* ($d_{p,VED}$ = 160 nm) of E1 using both "sphere" and "aggregate" representation. The yellow area in the figure represents the experimentally measured values, and the dashed line is the mean measured value for each case.

Further, the imaginary part of the refractive index m_{im} of bare BC was varied from 0.2 - 1 to study their dependence on the optical properties. Fig. 7(c) shows the SSA for the case III ($d_{p,\bar{V}}$ = 160 nm) of E1. The *SSA* calculated from the "sphere" representation is comparatively more sensitive to m_{im} than the results from the "aggregate" representation. The SSA from the "sphere" representation decreased as the m_{im} increases up to 0.5, after which there was an increase in the SSA. Whereas, the SSA calculated from the "aggregate" representation decreased steadily with m_{im}. It is observed that the modelled SSA is in good agreement with the measured results using the "aggregate" representation when m_{im} is between 0.3 - 1. In the "aggregate" representation, the *AAE* shows minimal sensitivity to m_{im} (Fig. 7d). It was found that the modelled results calculated using m_{im} between 0.50 - 1 fall close to the measured AAE. It was observed that spherical particles exhibit higher sensitivity than aggregate particles in the case of m_{im} as well.

He et al., 2015 demonstrated that the optical cross-sections of BC aggregates can vary up to 60% due to changes in the refractive indices. In this study, the sensitivity of optical properties modelled using spherical representation towards refractive indices were much higher. However, in the case of the "aggregate" representation, the sensitivities of the SSA and AAE of BC towards refractive indices was similar to that reported by He et al. (2015). Moreover, it must be noted that nature of dependencies of the optical properties towards m_{re} and m_{im} varied according to the morphology of BC chosen.

3.2.2 Fractal dimension

In this section, the sensitivity of the modelled results towards fractal dimension D_f is studied. As discussed in section 2.1, soot particles can have a wide range of D_f depending on the source of combustion, chemistry during formation, and the atmospheric conditions. A comparison of modelled and measured values is conducted to determine whether using the assumption of D_f as 1.7 in this study was accurate.

Figure 8 shows the modelled SSA (a to d) and AAE (e to f) as a function of D_f. The results were modelled using both monodisperse and polydisperse method for "aggregate" representation. The fractal dimension D_f was varied between 1.5 to 2.8 for cases *I* – *IV* of E1. Fig 8(a-d) shows that the SSA calculated with the polydisperse method changes by 20% with D_f, as also shown by Smith and Grainger (2014). However, it can be seen that the SSA is insensitive to D_f in the case of smaller soot particles with a $d_{p,\bar{V}}$ of 60 nm. In contrary, the results from the polydisperse method showed a variability of up to 100% with D_f. The SSA calculated at D_f between 1.7 - 1.9 was in good agreement with the average measured SSA for cases II – IV (Fig. 8b-d). Therefore, our assumption of D_f of 1.7 is a reasonably good choice for non-mature soot, like the ones formed from laboratory-based soot

https://doi.org/10.5194/egusphere-2022-573
Preprint. Discussion started: 2 August 2022

generators. Similarly, Fig. 8(e-h) shows the modelled AEE for D_f varying between 1.5 to 2.8. In the case of smaller soot particles with a $d_{p,\bar{V}}$ of 60 – 106 nm, the AAE was insensitive to D_f for both polydisperse and monodisperse method (Fig. 10a and 10b). For larger particles, the AAE varied up to 13% with changes in D_f (Fig. 8g and 8h). Overall, the SSA showed a higher dependency on the D_f, as compared to the AAE.

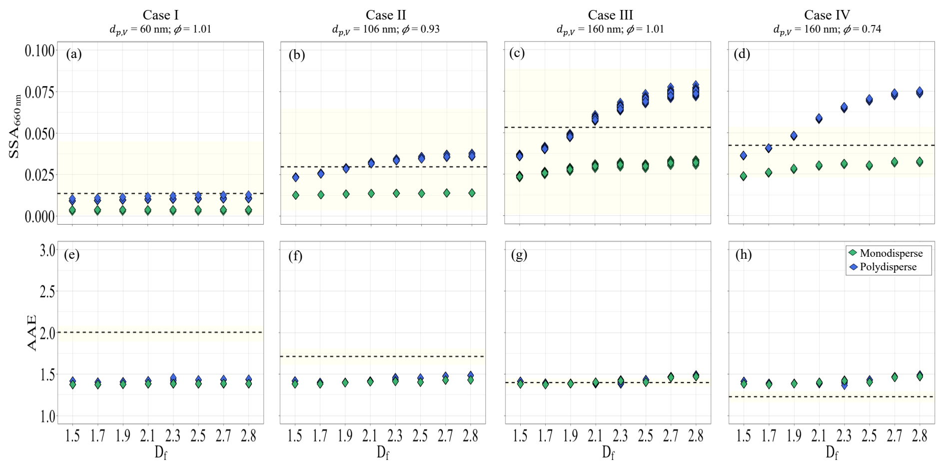

Figure 8. Sensitivity analysis of the modelled SSA and AEE using the "aggregate" representation. The fractal dimension D_f was varied between 1.5 to 2.8 for cases I – IV of E1, modelling the SSA **(a to d)** and AEE **(e to f).** The experimentally measured values are highlighted by the yellow area in the figure, and the dashed line represents the mean measured SSA or AAE for each case.

3.2.3 Primary particle radius

In Figure 9, the sensitivity of the optical properties to the primary particle radius a_{pp} was studied. The results were modelled using both monodisperse and polydisperse method for "aggregate" representation. The $a_{pp}$was varied between 5 to 28 nm for cases I – IV of E1, modelling the SSA (Fig.9, a-d) and AEE (Fig.9, e-f). He at al. (2014) reported that the optical cross sections of BC aggregates were not sensitive towards the size of their primary particles. However, the results in Fig. 9 showed that the SSA varied by up to a factor of 3 when the a_{pp} was changed between 5 and 28 nm for the monodisperse method. The difference increased up to 6, when the SSA was modelled using the polydisperse method. Therefore, the polydisperse method is more sensitive to a_{pp} as compared to monodisperse method. As compared to dependency of AAE towards D_f (Fig. 8), the AAE was observed to be more sensitive to a_{pp}. Except for the case III, the "aggregate" representation was not able to reproduce the measured AAE results. The possible reasons for discrepancies in modelled AAE was discussed in detail in Sec. 3.1.2. It is shown that for an a_{pp} value between 10 and 14 nm, the modelled SSA is in good agreement with the measured SSA for all cases, and is therefore, recommended for use in future studies.

https://doi.org/10.5194/egusphere-2022-573
Preprint. Discussion started: 2 August 2022

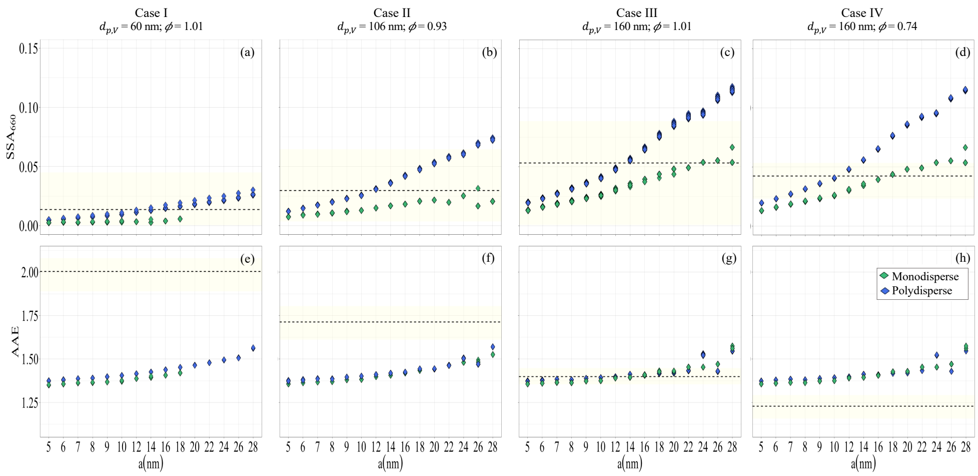

Figure 9. Sensitivity analysis of the modelled SSA and AEE using the "aggregate" representation. The primary particle radius $a_{pp}$was varied between 5 to 28 nm for cases I – IV of E1, modelling the SSA **(a to d)** and AEE **(e to f).** The experimentally measured values are highlighted by the yellow area in the figure, and the dashed line represents the mean measured SSA or AAE for each case. There are missing points in **(a)** and **(e)** of the monodisperse method results, which indicates that the particles are too small to form an aggregate with a_{pp} > 18 nm.

3.3 Experiment E2 - modelling techniques for BC with organics

In this section, the results of modelling BC particles with organics are discussed. The optical properties of BC particles generated from experiment E2 were modelled, and compared with their corresponding measured values. Figure 10 shows the results of the modelled SSA for various cases of the mini-CAST generators listed in Table 1. For each case of E2, the SSA was modelled using four representations of BC particles with organics: "coated sphere", "homogeneously mixed sphere", "coated aggregate", and "aggregate and sphere". Further, the SSA is modelled for both polydisperse and monodisperse methods.

In the case of mini-CAST 5201BC and 5303C (Fig. 10a, 10d, 10c, and 10f), the SSA modelled using the "coated aggregate", and "aggregate and sphere" representations for all the size methods agreed well with the measured SSA. However, for one of the cases of mini-CAST 5203C (Fig. 12e), the results of "coated aggregate", and "aggregate and sphere" representations underestimated the SSA. It was noted that the sensitivities to the various representations become comparatively less prominent in the case of smaller particle size (Fig. 10b, $d_{p,\overline{V}}$ = 86 nm, for mini-CAST 5203C).

In all the cases of E2, the monodisperse method (with $d_{p,\overline{V}}$) and polydisperse method of "coated sphere" and "homogeneously mixed sphere" representations overestimated the SSA by up to a factor of 3. Overall, the SSA modelled using the "coated aggregate" representation matched the measured values most closely, with a maximum deviation of 20% in certain cases. In the theoretical study by Liu et al. (2018), it was observed that the sensitivity of various representation of coated soot towards their absorption cross-section was varying with the size of the BC particle and the wavelength. A similar variation in the sensitivities of representations was seen in our results, e.g., for the cases of mini-CAST 5203C with $d_{p,\overline{V}}$ equal to 86 and 174 nm (Fig. 10b and 10e), changes in the behavior of the modelled SSA was notable. In Fig. 10b, when the particle is smaller in size, the SSA calculated for the "sphere and aggregate" representation using the monodisperse method is higher than that for the polydisperse method. In contrast, in Fig. 10e, when the particle is larger, the SSA calculated from the polydisperse method is larger.

The SSA calculated using the "aggregate and sphere" representation showed comparable results to that calculated using the "coated aggregate" representation. Laboratory-generated soot is less likely to resemble the "aggregate and sphere" depiction since the organic mass is evenly distributed around the BC aggregate. The "aggregate and sphere" representation usually depicts an aged soot particle where the BC aggregate is entirely encapsulated in a sphere of coating. Therefore, it is expected that using the "aggregate and sphere" for laboratory-generated soot would create a lensing effect, simulating higher absorption. However, because the coating accounted for less than 70% of the total particle volume, in none of our cases the coating encapsulated the

https://doi.org/10.5194/egusphere-2022-573
Preprint. Discussion started: 2 August 2022

aggregate. When the volume of coating is larger in laboratory-generated soot, using the "aggregate and sphere" representation may overestimate the absorption because of the lensing effect.

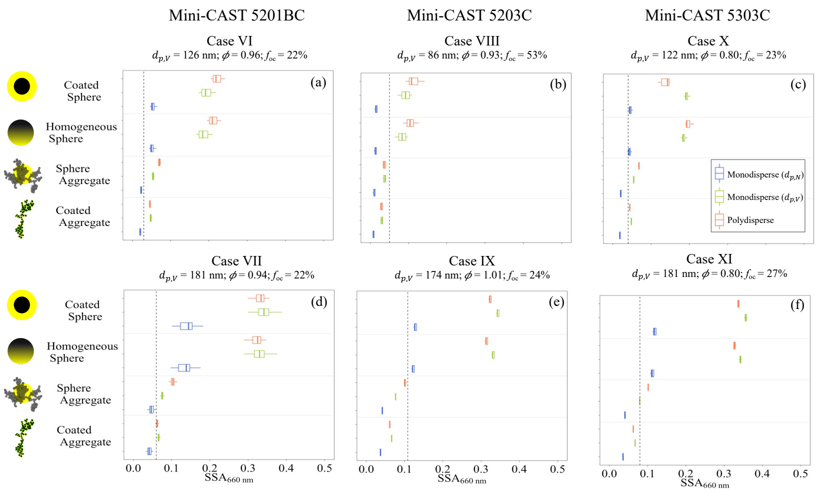

Figure 10. Modelled SSA at a wavelength of 660 nm from various cases of mini-CAST generators in E2 summarized in Table 1. The results are shown for: mini-CAST 5201BC $d_{p,\bar{V}}$ = 126 nm **(a);** mini-CAST 5201BC $d_{p,\bar{V}}$ = 181nm **(d);** mini-CAST 5203C $d_{p,\bar{V}}$ = 86 nm **(b);** mini-CAST 5203C $d_{p,\bar{V}}$ = 174 nm **(e);** mini-CAST 5303C $d_{p,\bar{V}}$ = 122 nm **(c);** mini-CAST 5303C $d_{p,\bar{V}}$ = 181 nm **(f).** In each panel, the SSA is modelled using four coated BC representations "coated sphere", "homogeneously mixed sphere", "coated aggregate", and "aggregate and sphere". Further, for each representation the SSA is modelled using monodisperse and polydisperse method. The mean of the experimentally measured SSA is shown by the black dashed line in each panel.

Figure 11 shows the modelled asymmetry parameter g for three cases of mini-CAST 5201BC. For each case, the g was modelled using the four representations of coated BC i.e., "coated sphere", "homogeneously mixed sphere", "coated aggregate", and "aggregate and sphere". Further in each of the representation, the g was calculated for monodisperse method (with $d_{p,\bar{N}}$ and $d_{p,\bar{V}}$). It was observed that the value of g increased as the coated BC particle grow in size, indicating more forward scattering for larger BC particles (Fig. 11a to 11c). However, the rate of increase of forward scattering with growing BC particles was more evident in the aggregate representations ("coated aggregate", and "aggregate and sphere"). Due to lack of experimental measurement of g, the modelled results could not be validated with the modelled findings.

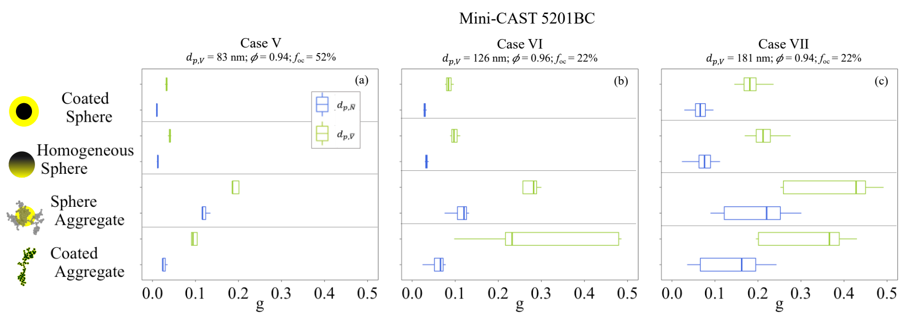

Figure 11. Asymmetry parameter g modelled using the four representations of coated BC i.e., "coated sphere", "homogeneously mixed sphere", "coated aggregate", and "aggregate and sphere". For each representation, the g is modelled using monodisperse particles (with $d_{p,\bar{N}}$ and $d_{p,\bar{V}}$). The results are shown for E2 cases V – VII: mini-

https://doi.org/10.5194/egusphere-2022-573
Preprint. Discussion started: 2 August 2022

CAST 5201BC $d_{p,\bar{V}}$ = 83 nm **(a);** mini-CAST 5201BC $d_{p,\bar{V}}$ = 126 nm **(b);** and mini-CAST 5201BC $d_{p,\bar{V}}$ = 181 nm **(c)**.

Figure 12 shows the BC mass absorption cross-sections (MAC_{BC}) modelled for three different cases of mini-CAST 5201BC ($d_{p,\bar{V}}$ = 83, 126, and 181 nm). In each case, MAC_{BC} is modelled using the four representations of coated BC i.e., "coated sphere", "homogeneously mixed sphere", "coated aggregate", and "aggregate and sphere". Forestierti et al. (2018) found that the spherical assumption used in the Lorentz-Mie theory underestimates the modelled mass absorption cross-sections (MAC_{BC}) for bare flame-generated soot. Figure 12a ($d_{p,\bar{V}}$ = 83 nm, and f_{oc}= 64%) shows that the MAC_{BC} calculated using spherical and aggregate representations underestimated the MAC_{BC}, consistent with Forestierti et al. (2018). However, for larger $d_{p,\bar{V}}$, the spherical representations overestimated the MAC_{BC} (Fig. 14b and 14c). In general, for larger particles, the modelled MAC_{BC} and measured MAC_{BC} were in better agreement when using "coated aggregate" representation.

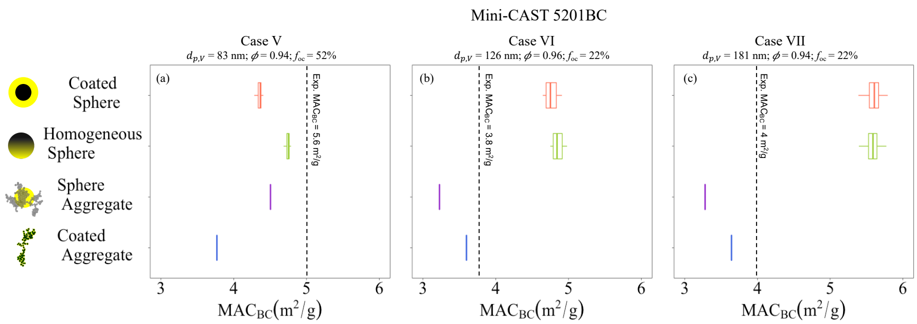

Figure 12. Black carbon mass absorption cross-section (MAC_{BC}) modelled using the four representations of coated BC i.e., "coated sphere", "homogeneously mixed sphere", "coated aggregate", and "aggregate and sphere". The results are shown E2 cases V – VII*:* mini-CAST 5201BC $d_{p,\bar{V}}$ = 83 nm **(a);** mini-CAST 5201BC $d_{p,\bar{V}}$ = 126 nm **(b);** and mini-CAST 5203C $d_{p,\bar{V}}$ = 181 nm **(c)**.

4 Conclusions

This work investigates the various modelling techniques for the optical properties of soot; and based on the results, recommendations for representing the morphology and size of soot are provided to the scientific community. The main goal of this study is to validate the different modelling approaches; therefore, the modelled optical properties were compared to measurements from laboratory-generated soot. The study is divided into two parts: (1) modelling techniques for bare BC – experiment E1; and (2) modelling techniques for BC with organics – experiment E2.

The laboratory experiment E1 was designed in such a way as to provide us with data to study modelling approaches for bare BC particles. The soot particles were generated under three conditions: the Catalytic Stripper was operated at unheated condition, at 150°C condition (BC particles pass through the Catalytic Stripper operated at 150°C), and at 350°C condition (BC particles pass through the Catalytic Stripper at 350°C). The aerosol generated when the Catalytic Stripper is operated at 350°C is expected to have the lowest organic content, therefore, this condition was considered most suitable for modelling the optical properties of bare BC.

For modelling the optical properties of bare BC, the two morphological representations "sphere" and "aggregate" were compared. Further for each morphological representation of bare BC, the optical properties were modelled using two size representations/methods: for monodisperse particles (monodisperse method), and for polydisperse particles (polydisperse method). In the case of monodisperse particles, the SSA modelled using "sphere" representation was higher than the measured value, which pronounces as the particle size increases. On the contrary, when using the "aggregate" representation, the modelled *SSA* results were in very good agreement with the measured SSA. In the case of polydisperse particles, the modelled optical properties (σ_{abs} and SSA) from the "aggregate" method were also in excellent agreement with the measured optical properties. Moreover, it was shown that the discrepancies between modelled and laboratory measured absorption can be reduced to 10%, when the polydisperse method, and an "aggregate" representation of BC is used. These results confirm that the mini-CAST generated soot particles are indeed fractal-like as also shown by TEM images (Ess et al., 2021; Mamakos et al., 2013) and "aggregate" representation of BC is recommended to be used when modelling their optical properties (σ_{abs} and SSA).

However, in contrast to the results of σ_{abs} and SSA, the AAE modelled using the "aggregate" representation vary from the measured AAE by a factor of 1.5. In the case of larger particles (≥100 nm), the modelled AAE from the "sphere" representation were in better agreement with the measured results. For smaller BC particles, both the "sphere" and "aggregate" representations underestimated the AAE. Possibly, the soot particles are solid agglomerates at smaller sizes, but they are not yet fully carbonized, and some non-volatile organic content is embedded in the soot structure (Maricq, 2014). Furthermore, smaller particles contain more organic content than larger ones (Zhang et al., 2020), leading to a less effective removal by Catalytic Stripper. In the case that the smaller particles were immature solid soot with embedded organic content, the assumption that they are bare may account for the underestimation of modelled AAE in comparison to measured values.

After studying the various size and morphological representations for modelling bare BC particles, the assumptions of various modelling parameters (for e.g., m_{re}, m_{im}, D_f, and a_{pp}) were evaluated. The sensitivity of the modelled optical properties (SSA and AAE) to the real and the imaginary part of the refractive index (m_{re} and m_{im}) was studied. It is shown that the nature of dependency of the optical properties towards m_{re} and m_{im} varies according to the morphological representation used. For e.g., the modelled SSA was highly sensitive to the m_{re}, varying by up to a factor of 2.5. In the same case, the modelled SSA did not depend as strongly on m_{re} in the aggregate morphological representation. The modelled optical properties of BC were well aligned with measured values when using the aggregate morphological representation and assumptions of refractive indices as: (i) m_{re} between 1.6 to 2; and (ii) m_{imag} between 0.50 to 1.

Since our analysis indicated using aggregate morphological representations of soot tends to provide more accurate optical properties, their sensitivity to two key aggregate parameters (fractal dimension D_f and primary particle radius a_{pp}) were investigated. In the case of polydisperse particles, the modelled SSA showed a variability of up to 100% with changes in the D_f. Although, in smaller BC particles, the SSA was insensitive to changes in the D_f because of the underdeveloped aggregate structure. The AAE was rather less sensitive to the changes in the D_f for both the monodisperse and polydisperse methods. When studying the modelled SSA as a function of primary particle radius, it was observed that the SSA varied by a factor of 3 and 6, for the monodisperse and polydisperse particles, respectively. To conclude, a good agreement was found between the modelled and experimentally measured optical properties of BC when: (i) D_f from 1.7 to 1.9, and (ii) a_{pp} between 10 to 14 nm.

In order to study the modelling approaches for coated BC particles, three kinds of mini-CAST soot generators were used to produce soot particles with organic carbon content between 35 - 65%. Four kinds of morphological representations for coated BC (two each for spherical and aggregate) were compared using both monodisperse and polydisperse particles. In the most of the results, the modelled SSA using the "coated aggregate" and "aggregate and sphere" representation was in good agreement with the measured SSA. Though it is less likely that laboratory-generated soot will resemble the "aggregate and sphere" representation, it can still be used when the coating only makes up a small part of the total particle volume. Therefore, our results show that for coated soot particles as well, the aggregate morphological representation gives more accurate modelled optical properties. Moreover, when polydisperse method is used the accuracy improves by up to a factor of 2. These results in combination emphasize on the importance of morphology and size representation while modelling optical properties of soot particles.

This study provides experimental support for previous theoretical work based on BC as fractal aggregates (e.g., Kahnert, 2010; Adaichi et al., 2010; Kahnert and Kanngießer, 2020; Smith and Grainger, 2014; Romshoo et al., 2021; Liu et al., 2019; Luo et al., 2018). Analysis of various modelling methods for BC particles showed that the selection of an appropriate size representation (polydisperse size method) and an appropriate morphological representation (aggregate morphology) could result in a more realistic prediction of BC's optical properties (σ_{abs} and SSA). Although optical simulations are time-consuming, it is suggested to use polydisperse size method for future modelling studies of BC fractal aggregates. The long-term goal should be to incorporate aggregate morphological representation during black carbon parametrization scheme development and application to global climate models. The findings of this study are an good example of how parallel measurements and modelling research can reduce the uncertainties in optical properties of BC. Future investigations could compare optical modelling results of BC to ambient atmospheric measurements, in order to reduce the uncertainties as a result of their complex aging process.

Appendix A: Experimental setup and instrumentation

Figure A1 shows an overview of the experimental setup used in experiment E1: measurements of thermally denuded nascent soot particles. The pre-treated particles were divided into four aerosol flows (i.e. sampling lines) and delivered to the different instruments. One part of the aerosol flow passed through a Mobility Particle Size Spectrometer (MPSS, TROPOS design; sample flow rate of 1 lpm; Wiedensohler et al., 2012; 2018) which measured the particle number size distribution of the soot particles. Another part of the aerosol flowed was guided to a Cavity Attenuated Phase Shift Extinction monitor (CAPS $PM_{ex\ 630}$, Aerodyne Res. Inc., USA; flow rate of 1 lpm) which measured the light extinction coefficient, σ_{sca} at wavelength of 630 nm. The other part of the aerosol

https://doi.org/10.5194/egusphere-2022-573
Preprint. Discussion started: 2 August 2022

flow entered an aethalometer (AE33 Aethalometer, Magee Scientific, Berkeley, USA; flow rate of 5 lpm) which monitored the equivalent black carbon concentration at seven wavelengths between 370 and 950 nm. The equivalent black carbon concentration was converted into the aerosol light absorption coefficient (σ_{abs}), as described in Müller et al. (2011). A further part of the aerosols was passed through a nephelometer (Aurora 4000, Ecotech Pvt Ltd, Melbourne, Australia) and a multi-angle absorption photometer (MAAP, type 5012, Thermo Scientific, Franklin, MA) running in tandem configuration at a flow rate of 10 lpm that measured the particle light scattering coefficient, σ_{scat}, and the absorption coefficients, σ_{abs} , respectively. The σ_{abs} obtained from the AE33 was corrected by a factor of 0.95 to 1.3 to match the σ_{abs} from MAAP. The σ_{scat} measured from the nephelometer was also corrected for truncation errors due to the finite viewing angle of the detector, given in detail by Müller et al. (2009).

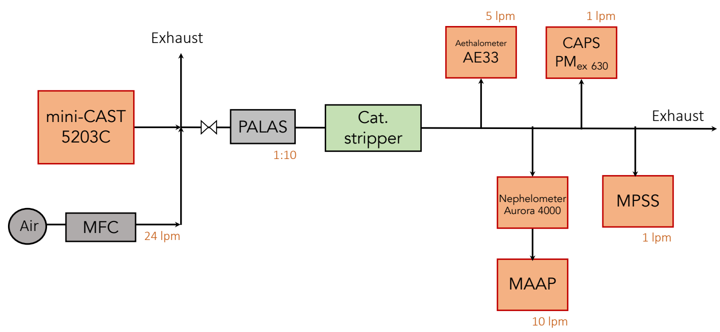

Figure A1. Experimental setup of E1: generation and measurements of denuded BC particles. The soot generator mini-CAST 5203C was used to generate the particles under different operating conditions given in Table 1. A mass flow controller (MFC) was used to mix the aerosols generated from mini-CAST 5203C with air, and then a Catalytic Stripper at 350°C was used to remove the volatile contents. The heated soot particles were divided into four aerosol flows and delivered to instruments. The different instruments measuring the physical and optical properties are Mobility Particle Size Spectrometer (MPSS), Cavity Attenuated Phase Shift Extinction monitor (CAPS $PM_{ex\ 630}$), aethalometer (AE33), nephelometer, and multi-angle absorption photometer (MAAP).

Figure A2 shows a schematic diagram of the experimental setup used in E2: measurements of untreated nascent soot particles. The aerosol from the mini-CAST using a dilution system (PALAS VKL 10, PALAS, Karlsruhe, Germany) was fed into the mixing chamber and delivered to various measurement systems through several sampling ports. The aerosol from the first sampling port flowed at 6 lpm into a nephelometer (Aurora 4000) and a multi-angle absorption photometer (MAAP, type 5012) arranged in tandem configuration. The aerosol from a second port was guided to an Aethalometer (AE33; flow rate of 8 lpm), and three Cavity Attenuated Phase Shift Extinction monitor: CAPS $PM_{ex\ 450}$, CAPS $PM_{ex\ 530}$, and CAPS $PM_{ex\ 630}$ (flow rate of 8 lpm), which measured at wavelengths of 450, 530, and 630 nm, respectively. Subsequently, the aerosol flowed into the MPSS (TROPOS design; flow rate of 1 lpm) and the Cavity Attenuated Phase Shift single scatter albedo monitor (CAPS $PM_{SSA\ 630}$, Aerodyne Res. Inc., USA; flow rate of 1lpm) from the third and fourth sampling port, respectively. The CAPS $PM_{SSA\ 630}$ measured the scattering coefficient, σ_{sca}, and the extinction coefficient, σ_{ext} at a wavelength of 630 nm. Through the fourth port, the aerosol mass concentration was determined by using the Tapered Element Oscillating Microbalance (TEOM 1405, Thermo Scientific, Franklin, MA; flow rate of 3 lpm). The aerosol from the last port was sampled on quartz fibre filters at a flow rate of 2-3 lpm and subsequently analysed by a EC/OC analyser (Sunset Laboratory Inc., Hillsborough, USA). The loaded quartz fibre filters were analysed at different laboratories, including METAS (Switzerland) and NPL (UK). For a better overview, the details of the instrumentation used in E1 and E2 laboratory experiments are summarized in Table A1.

https://doi.org/10.5194/egusphere-2022-573
Preprint. Discussion started: 2 August 2022

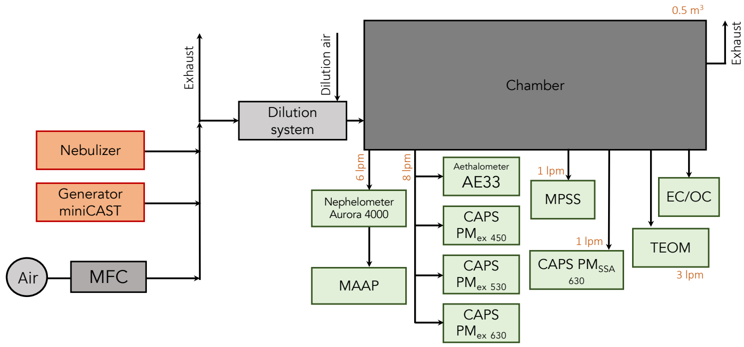

Figure A2. Experimental setup of E2: generation and measurements of BC particles with organics. The soot particles are generated using different mini-CAST generators operated under flow settings given in Table 1. Mini-CAST soot generators produce aerosols that are mixed with air from the mass flow controller (MFC). After passing through a dilution system, the aerosols enter the mixing chamber. The soot particles are delivered to various instruments measuring physical, optical, and chemical properties. The instruments used in this experiment are the aethalometer (AE33), nephelometer, multi-angle absorption photometer (MAAP), Cavity Attenuated Phase Shift Extinction monitor (CAPS $PM_{ex\ 630}$), a Cavity Attenuated Phase Shift Extinction monitor (CAPS $PM_{ex\ 530}$), Cavity Attenuated Phase Shift Extinction monitor (CAPS $PM_{ex\ 450}$), Cavity Attenuated Phase Shift single scatter albedo monitor (CAPS $PM_{SSA\ 630}$), Mobility Particle Size Spectrometer (MPSS), and Tapered Element Oscillating Microbalance (TEOM).

Table A1. Details of the instruments used in E1 and E2.

Instrument	Manufacturer	Function or measured variable	Experiment
mini-CAST 5203 Type C	Jing	Soot generator	E1, E2
mini-CAST 5201 Type BC	Jing	Soot generator	E2
mini-CAST 5303 Type C	Jing	Soot generator	E2
Mobility Particle Size Spectrometer (MPSS)	TROPOS	Particle number size distribution (Mobility diameter)	E1, E2
Cavity Attenuation Phase Shift Spectrometer (CAPS $PM_{ex\ 630}$)	Aerodyne Research	Particle light extinction coefficients (σ_{ext}) in Mm^{-1} at λ = 630 nm	E1, E2
Cavity Attenuation Phase Shift Spectrometer (CAPS $PM_{ex\ 530}$	Aerodyne Research	Particle light extinction coefficients (σ_{ext}) in Mm^{-1} at λ = 530 nm	E2
Cavity Attenuation Phase Shift Spectrometer (CAPS $PM_{ex\ 450}$	Aerodyne Research	Particle light extinction coefficients (σ_{ext}) in Mm^{-1} at λ = 450 nm	E2
Cavity Attenuation Phase Shift Spectrometer (CAPS $PMssa_{630}$	Aerodyne Research	Particle light scattering and extinction coefficients at Mm^{-1} at λ = 630 nm	E2
Aethalometer AE33	Magee Scientific	Particle light absorption coefficients (σ_{abs}) in Mm^{-1} at seven wavelength, λ = 370, 470, 520, 590, 660, 880, and 950 nm	E1, E2
Multi-angle absorption photometer (MAAP)	Thermo-Scientific	Particle light absorption coefficients (σ_{abs}) in Mm^{-1} at 637 nm	E1, E2
Tapered Element Oscillating Microbalance (TEOM)	Thermo-Scientific	Particle mass concentration	E2
Nephelometer	Aurora	Particle light scattering coefficients (σ_{sca}) in Mm^{-1} at 635 nm	E1, E2

https://doi.org/10.5194/egusphere-2022-573
Preprint. Discussion started: 2 August 2022

Appendix B: Details about modelling

The first method for calculation of number of primary particles per aggregate (N_{pp}) from the $d_{p,\bar{N}}$ (Rissler et al. 2012; Bladh et al. 2001) is given as:

$$N_{pp}(d_{p,\bar{N}}) = \frac{m_{agg}(d_{p,\bar{N}})}{m_{pp}(d_{p,\bar{N}})} = \frac{\frac{{d_{p,\bar{N}}}^3}{2} \cdot \rho_{eff}}{{R_{pp}}^3 \cdot \rho_{pp}}, \tag{B1}$$

where the mass of the aggregate m_{agg} was assumed to have an effective density ρ_{eff} (g/cm^3), and the mass of the primary particle is m_{pp} was assumed to have a density ρ_{pp} of 1.8 g/cm^3 (Rissler et al. 2013). Following the study of Malik et al. 2011, the ρ_{eff} was assumed as 0.76 ± 0.04 g/cm^3 for $d_{p,\bar{N}}$ < 50nm, and for 250 < $d_{p,\bar{N}}$ < 50 nm, the ρ_{eff} was 0.51 ± 0.04 g/cm^3.

The second method developed by Sorensen (2011) is applicable to black carbon fractal aggregates since they are formed by the Diffusion Limited Aggregation DLA process and fall under the slip regime. Slip regime is a transition between the continuum and free molecular regime, where the Knudsen number Kn lies between 0.1 to 10. The Knudsen number Kn is the ratio of the molecular free path to the aggregate mobility radius (Friedlander 2000). The conversion is given as:

$$d_{p,\bar{N}} = 2R_{pp} \cdot {N_{pp}}^{0.46} \quad N_{pp} < 100\,, \tag{B2}$$
$$d_{p,\bar{N}} = 2R_{pp} \cdot (10^{-2x+0.92}) \cdot {N_{pp}}^{x} \quad N_{pp} > 100\,, \tag{B3}$$

with a mobility mass scaling exponent of $x = 0.51Kn^{0.043}$ for 0.46 < x < 0.56. In this study, the average value of the mobility mass scaling exponent x = 0.51 ± 0.02 was assumed.

The third method, developed by Schmidt-Ott. (1988) follows a power law function, and is given as:

$$N_{pp} = K \cdot \left(\frac{d_{p,\bar{N}}}{2R_{pp}}\right)^{D_{fm}}, \tag{B4}$$

where, K is a pre-factor, D_f is the fractal dimension, and D_{fm} is the mass mobility exponent. According to Park, Kittelson, & McMurry (2004) the relation between D_{fm} and D_f is $D_{fm} = 1.26 \cdot D_f$ for diesel soot, which was also used in this study. The value of D_f was taken from literature. For all the three conversion methods, the N_{pp} was estimated using both the number mean mobility diameter ($d_{p,\bar{N}}$), and the volume mean mobility diameter ($d_{p,\bar{V}}$).

Table B1. Values of m_{re} and m_{im} used in this study (Kim et al., 2015) for elemental carbon (EC) and organic carbon (OC).

Refractive index (m)	Wavelength (nm)		
	467	530	660
Elemental carbon (EC)			
m_{re}	1.92	1.96	2.0
m_{im}	0.67	0.65	0.63
Organic carbon (OC)			
m_{re}	1.59	1.47	1.47
m_{im}	0.11	0.04	0

Appendix C: Symbols and acronyms

Table C1. Symbols used.

Symbol	Meaning
σ_{ext}	Extinction coefficient
σ_{abs}	Absorption coefficient
σ_{sca}	Scattering coefficient
Q_{ext}	Extinction efficiency
Q_{abs}	Absorption efficiency
Q_{sca}	Scattering efficiency

https://doi.org/10.5194/egusphere-2022-573
Preprint. Discussion started: 2 August 2022

g	Asymmetry parameter
m_{re}	Real part of refractive index
m_{im}	Imaginary part of refractive index
D_f	Fractal dimension
N_{pp}	Number of primary particles in aggregate
a_{pp}	Radius of a primary particle (no coating)
a_{in}	Inner radius of a primary particle (with coating)
a_o	Outer radius of a primary particle (with coating)
D_{in}	Inner diameter of volume equivalent sphere
D_o	Outer diameter of volume equivalent sphere
d_p	Mobility diameter
$d_{p,\bar{N}}$	Number mean mobility diameter
$d_{p,\bar{V}}$	Volume mean mobility diameter
ϕ	Flame equivalence ratio
f_{oc}	Fraction of organic carbon
D_i	Diameter of i^{th} SMPS size bin
n_i	Number concentration of i^{th} SMPS size bin
Q_{abs_i}	Absorption efficiency of i^{th} SMPS size bin
C_{abs_i}	Absorption cross-section of i^{th} SMPS size bin

Table C2. Acronyms used.

Acronym	Meaning
BC	Black carbon
SSA	Single scattering albedo
MAC_{BC}	Mass absorption cross-section
AAE	Ångström absorption exponent

Acknowledgement

This work is supported by the 16ENV02 Black Carbon project of the European Union through the European Metrology Programme for Innovation and Research (EMPIR).

Code availability

The Python Mie scattering package is available at https://pymiescatt.readthedocs.io/en/latest/index.html#. The software used to generate the fractal aggregates is available at https://sites.google.com/view/fabriceonofri/aggregates/fractal-like-aggregates-diffusion-model. The code for the multi-sphere T-matrix (MSTM) method used in this manuscript is publicly available at https://eng.auburn.edu/users/dmckwski/scatcodes/.

Data availability

The data obtained from this study are available upon request from the corresponding author (baseerat@tropos.de).

References

Abel, S. J., Haywood, J. M., Highwood, E. J., Li, J. and Buseck, P. R.: Evolution of biomass burning aerosol properties from an agricultural fire in southern Africa, Geophysical Research Letters, 30(15), doi:10.1029/2003GL017342, 2003.

Adachi, K., Chung, S. H. and Buseck, P. R.: Shapes of soot aerosol particles and implications for their effects on climate, Journal of Geophysical Research Atmospheres, 115(15), doi:10.1029/2009JD012868, 2010.

Berry, M. V. and Percival, I. C.: Optics of fractal clusters such as smoke, Optica Acta, 33(5), 577–591, doi:10.1080/713821987, 1986.

Betrancourt, C., Liu, F., Desgroux, P., Mercier, X., Faccinetto, A., Salamanca, M., Ruwe, L., Kohse-Höinghaus, K., Emmrich, D., Beyer, A., Gölzhäuser, A. and Tritscher, T.: Investigation of the size of the incandescent incipient soot particles in premixed sooting and nucleation flames of n-butane using LII, HIM, and 1 nm-SMPS, Aerosol Science and Technology, 51(8), 916–935, doi:10.1080/02786826.2017.1325440, 2017.

Bladh, H., Johnsson, J., Rissler, J., Abdulhamid, H., Olofsson, N. E., Sanati, M., Pagels, J. and Bengtsson, P. E.: Influence of soot particle aggregation on time-resolved laser-induced incandescence signals, in Applied Physics B: Lasers and Optics, vol. 104, pp. 331–341., 2011.

Bohren, C. F. and Huffman, D. R.: Absorption and Scattering of Light by Small Particles., 1998.

Bond, T. C. and Bergstrom, R. W.: Light absorption by carbonaceous particles: An investigative review, Aerosol Science and Technology, 40(1), 27–67, doi:10.1080/02786820500421521, 2006.

Bond, T. C., Doherty, S. J., Fahey, D. W., Forster, P. M., Berntsen, T., Deangelo, B. J., Flanner, M. G., Ghan, S., Kärcher, B., Koch, D., Kinne, S., Kondo, Y., Quinn, P. K., Sarofim, M. C., Schultz, M. G., Schulz, M., Venkataraman, C., Zhang, H., Zhang, S., Bellouin, N., Guttikunda, S. K., Hopke, P. K., Jacobson, M. Z., Kaiser, J. W., Klimont, Z., Lohmann, U., Schwarz, J. P., Shindell, D., Storelvmo, T., Warren, S. G. and Zender, C. S.: Bounding the role of black carbon in the climate system: A scientific assessment, Journal of Geophysical Research Atmospheres, 118(11), 5380–5552, doi:10.1002/jgrd.50171, 2013.

Bourrous, S., Ribeyre, Q., Lintis, L., Yon, J., Bau, S., Thomas, D., Vallières, C. and Ouf, F. X.: A semi-automatic analysis tool for the determination of primary particle size, overlap coefficient and specific surface area of nanoparticles aggregates, Journal of Aerosol Science, 126, 122–132, doi:10.1016/j.jaerosci.2018.09.001, 2018.

Ciupek, K., Quincey, P., Green, D. C., Butterfield, D. and Fuller, G. W.: Challenges and policy implications of long-term changes in mass absorption cross-section derived from equivalent black carbon and elemental carbon measurements in London and south-east England in 2014–2019, Environmental Science: Processes & Impacts, 23(12), 1949–1960, doi:10.1039/d1em00200g, 2021.

Chylek, P. and Wong, J.: Effect of absorbing aerosols on global radiation budget, Geophysical Research Letters, 22(8), 929–931, doi:10.1029/95GL00800, 1995.

Eggersdorfer, M. L., Kadau, D., Herrmann, H. J. and Pratsinis, S. E.: Aggregate morphology evolution by sintering: Number and diameter of primary particles, Journal of Aerosol Science, 46, 7–19, doi:10.1016/j.jaerosci.2011.11.005, 2012.

Ess, M. N., Bertò, M., Irwin, M., Modini, R. L., Gysel-Beer, M. and Vasilatou, K.: Optical and morphological properties of soot particles generated by the mini-CAST 5201 BC generator, Aerosol Science and Technology, 55(7), 828–847, doi:10.1080/02786826.2021.1901847, 2021.

Ess, M. N. and Vasilatou, K.: Characterization of a new mini-CAST with diffusion flame and premixed flame options: Generation of particles with high EC content in the size range 30 nm to 200 nm, Aerosol Science and Technology, 53(1), 29–44, doi:10.1080/02786826.2018.1536818, 2019.

Fierce, L., Riemer, N. and Bond, T. C.: Explaining variance in black carbon"s aging timescale, Atmospheric Chemistry and Physics, 15(6), 3173–3191, doi:10.5194/acp-15-3173-2015, 2015.

Forestieri, S. D., Helgestad, T. M., Lambe, A. T., Renbaum-Wolff, L., Lack, D. A., Massoli, P., Cross, E. S., Dubey, M. K., Mazzoleni, C., Olfert, J. S., Sedlacek, A. J., Freedman, A., Davidovits, P., Onasch, T. B. and Cappa, C. D.: Measurement and modeling of the multiwavelength optical properties of bare flame-generated soot, Atmospheric Chemistry and Physics, 18(16), 12141–12159, doi:10.5194/acp-18-12141-2018, 2018.

Friedlander, S.: Smoke, dust and haze. Fundamentals of aerosol behaviour., , doi:10.1063/1.3037714, 1977.

Fuller, K. A., Malm, W. C. and Kreidenweis, S. M.: Effects of mixing on extinction by carbonaceous particles, Journal of Geophysical Research: Atmospheres, 104(D13), 15941–15954, doi:10.1029/1998JD100069, 1999.

Ghazi, R. and Olfert, J. S.: Coating mass dependence of soot aggregate restructuring due to coatings of oleic acid and dioctyl sebacate, Aerosol Science and Technology, 47(2), 192–200, doi:10.1080/02786826.2012.741273, 2013.

Gini, M. I., Helmis, C., Melas, A. D., Papanastasiou, D., Orfanopoulos, G., Giannakopoulos, K. P., Drossinos, Y. and Eleftheriadis, K.: Characterization of carbon fractal-like aggregates by size distribution measurements and theoretical calculations, Aerosol Science and Technology, 50(2), 133–147, doi:10.1080/02786826.2015.1134763, 2016.

Gwaze, P., Schmid, O., Annegarn, H. J., Andreae, M. O., Huth, J. and Helas, G.: Comparison of three methods of fractal analysis applied to soot aggregates from wood combustion, Journal of Aerosol Science, 37(7), 820–838, doi:10.1016/j.jaerosci.2005.06.007, 2006.

He, C., Liou, K. N., Takano, Y., Zhang, R., Levy Zamora, M., Yang, P., Li, Q. and Leung, L. R.: Variation of the radiative properties during black carbon aging: Theoretical and experimental intercomparison, Atmospheric Chemistry and Physics, 15(20), 11967–11980, doi:10.5194/acp-15-11967-2015, 2015.

Hergert, W. and Wriedt, T.: The Mie Theory: Basics and Applications., 2012.

IPCC, 2021: Summary for Policymakers. In: Climate Change 2021: The Physical Science Basis. Contribution of Working Group I to the Sixth Assessment Report of the Intergovernmental Panel on Climate Change [Masson-Delmotte, V., P. Zhai, A. Pirani, S.L. Connors, C. Péan, S. Berger, N. Caud, Y. Chen, L. Goldfarb, M.I. Gomis, M. Huang, K. Leitzell, E. Lonnoy, J.B.R. Matthews, T.K. Maycock, T. Waterfield, O. Yelekçi, R. Yu, and B. Zhou (eds.)]. In Press.

Jacobson, M. Z.: Strong radiative heating due to the mixing state of black carbon in atmospheric aerosols, Nature, 409(6821), 695–697, doi:10.1038/35055518, 2001.

Janssen, N. A. H., Hoek, G., Simic-Lawson, M., Fischer, P., van Bree, L., Brink, H. Ten, Keuken, M., Atkinson, R. W., Ross Anderson, H., Brunekreef, B. and Cassee, F. R.: Black carbon as an additional indicator of the adverse health effects of airborne particles compared with pm10 and pm2.5, Environmental Health Perspectives, 119(12), 1691–1699, doi:10.1289/ehp.1003369, 2011.

Jing, L., 2014, Instruction Manual of Real Soot Generator Model 5203 Type C mini-CAST. Jing Ltd

Kahnert, M. and Kanngießer, F.: Modelling optical properties of atmospheric black carbon aerosols, Journal of Quantitative Spectroscopy and Radiative Transfer, 244, doi:10.1016/j.jqsrt.2020.106849, 2020.

Kahnert, M.: Numerically exact computation of the optical properties of light absorbing carbon aggregates for wavelength of 200 nm-12.2 μm, Atmospheric Chemistry and Physics, 10(17), 8319–8329, doi:10.5194/acp-10-8319-2010, 2010.

Kholghy, M., Saffaripour, M., Yip, C. and Thomson, M. J.: The evolution of soot morphology in a laminar coflow diffusion flame of a surrogate for Jet A-1, Combustion and Flame, 160(10), 2119–2130, doi:10.1016/j.combustflame.2013.04.008, 2013.

Kim, J., Bauer, H., Dobovičnik, T., Hitzenberger, R., Lottin, D., Ferry, D. and Petzold, A.: Assessing optical properties and refractive index of combustion aerosol particles through combined experimental and modeling studies, Aerosol Science and Technology, 49(5), 340–350, doi:10.1080/02786826.2015.1020996, 2015.

Kirchstetter, T. W. and Novakov, T.: Controlled generation of black carbon particles from a diffusion flame and applications in evaluating black carbon measurement methods, Atmospheric Environment, 41(9), 1874–1888, doi:10.1016/j.atmosenv.2006.10.067, 2007.

Krüger, O. O., Holanda, B. A., Chowdhury, S., Pozzer, A., Walter, D., Pöhlker, C., Andrés Hernández, M. D., Burrows, J. P., Voigt, C., Lelieveld, J., Quaas, J., Pöschl, U., and Pöhlker, M. L.: Black carbon aerosol reductions during COVID-19 confinement quantified by aircraft measurements over Europe, Atmos. Chem. Phys. Discuss. [preprint], https://doi.org/10.5194/acp-2021-1100, in review, 2022.

Li, J., Liu, C., Yin, Y. and Kumar, K. R.: Numerical investigation on the Ångström exponent of black carbon aerosol, Journal of Geophysical Research, 121(7), 3506–3518, doi:10.1002/2015JD024718, 2016.

https://doi.org/10.5194/egusphere-2022-573
Preprint. Discussion started: 2 August 2022

Liu, C., Chung, C. E., Yin, Y. and Schnaiter, M.: The absorption Ångström exponent of black carbon: From numerical aspects, Atmospheric Chemistry and Physics, 18(9), 6259–6273, doi:10.5194/acp-18-6259-2018, 2018.

Liu, C., Li, J., Yin, Y., Zhu, B. and Feng, Q.: Optical properties of black carbon aggregates with non-absorptive coating, Journal of Quantitative Spectroscopy and Radiative Transfer, 187, 443–452, doi:10.1016/j.jqsrt.2016.10.023, 2017.

Liu, C., Xu, X., Yin, Y., Schnaiter, M. and Yung, Y. L.: Black carbon aggregates: A database for optical properties, Journal of Quantitative Spectroscopy and Radiative Transfer, 222–223, 170–179, doi:10.1016/j.jqsrt.2018.10.021, 2019.

Liu, L. and Mishchenko, M. I.: Scattering and radiative properties of morphologically complex carbonaceous aerosols: A systematic modeling study, Remote Sensing, 10(10), doi:10.3390/rs10101634, 2018.

Luo, J., Zhang, Y., Wang, F., Wang, J. and Zhang, Q.: Applying machine learning to estimate the optical properties of black carbon fractal aggregates, Journal of Quantitative Spectroscopy and Radiative Transfer, 215, 1–8, doi:10.1016/j.jqsrt.2018.05.002, 2018.

Mackowski, D. W. and Mishchenko, M. I.: A multiple sphere T-matrix Fortran code for use on parallel computer clusters, Journal of Quantitative Spectroscopy and Radiative Transfer, 112(13), 2182–2192, doi:10.1016/j.jqsrt.2011.02.019, 2011.

Mackowski, D. W.: A multiple sphere T-matrix FORTRAN code for use on parallel computer clusters, Version 3.0, Department of Mechanical Engineering Auburn University [code], Auburn, USA, available at: https://eng.auburn.edu/users/ dmckwski/scatcodes/, last access: 15 September 2020.

Madueño, L., Kecorius, S., Birmili, W., Müller, T., Simpas, J., Vallar, E., Galvez, M. C., Cayetano, M. and Wiedensohler, A.: Aerosol particle and black carbon emission factors of vehicular fleet in Manila, Philippines, Atmosphere, 10(10), doi:10.3390/atmos10100603, 2019.

Malik, A., Abdulhamid, H., Pagels, J., Rissler, J., Lindskog, M., Nilsson, P., Bjorklund, R., Jozsa, P., Visser, J., Spetz, A. and Sanati, M.: A potential soot mass determination method from resistivity measurement of thermophoretically deposited soot, Aerosol Science and Technology, 45(2), 284–294, doi:10.1080/02786826.2010.533214, 2011.

Mamakos, A., Khalek, I., Giannelli, R. and Spears, M.: Characterization of combustion aerosol produced by a mini-CAST and treated in a catalytic stripper, Aerosol Science and Technology, 47(8), 927–936, doi:10.1080/02786826.2013.802762, 2013.

Maricq, M. M.: Examining the relationship between black carbon and soot in flames and engine exhaust, Aerosol Science and Technology, 48(6), 620–629, doi:10.1080/02786826.2014.904961, 2014.

Menon, S., Hansen, J., Nazarenko, L. and Luo, Y.: Climate effects of black carbon aerosols in China and India, Science, 297(5590), 2250–2253, doi:10.1126/science.1075159, 2002.

Michelsen, H. A.: Probing soot formation, chemical and physical evolution, and oxidation: A review of in situ diagnostic techniques and needs, Proceedings of the Combustion Institute, 36(1), 717–735, doi:10.1016/j.proci.2016.08.027, 2017.

Mie, G.: On the optics of turbid media, especially colloidal metal solutions, Ann. Phys. Berlin, 25(3), 377–445, 1908.

Mishchenko, M. I., Travis, L. D. and Lacis, A. a: Scattering, Absorption, and Emission of Light by Small Particles, Vasa, 1–486, 2002.

Mishchenko, M. I., Liu, L., Travis, L. D. and Lacis, A. A.: Scattering and radiative properties of semi-external versus external mixtures of different aerosol types, Journal of Quantitative Spectroscopy and Radiative Transfer, 88(1–3), 139–147, doi:10.1016/j.jqsrt.2003.12.032, 2004.

Mishchenko, M. I., Travis, L. D. and Mackowski, D. W.: T-matrix computations of light scattering by nonspherical particles: A review, Journal of Quantitative Spectroscopy and Radiative Transfer, 55(5), 535–575, doi:10.1016/0022-4073(96)00002-7, 1996.

Moore, R. H., Ziemba, L. D., Dutcher, D., Beyersdorf, A. J., Chan, K., Crumeyrolle, S., Raymond, T. M., Thornhill, K. L., Winstead, E. L. and Anderson, B. E.: Mapping the operation of the miniature combustion aerosol standard (Mini-CAST) soot generator, Aerosol Science and Technology, 48(5), 467–479, doi:10.1080/02786826.2014.890694, 2014.

Müller, T., Henzing, J. S., De Leeuw, G., Wiedensohler, A., Alastuey, A., Angelov, H., Bizjak, M., Collaud Coen, M., Engström, J. E., Gruening, C., Hillamo, R., Hoffer, A., Imre, K., Ivanow, P., Jennings, G., Sun, J. Y., Kalivitis, N., Karlsson, H., Komppula, M., Laj, P., Li, S. M., Lunder, C., Marinoni, A., Martins Dos Santos, S., Moerman, M., Nowak, A., Ogren, J. A., Petzold, A., Pichon, J. M., Rodriquez, S., Sharma, S., Sheridan, P. J., Teinilä, K., Tuch, T., Viana, M., Virkkula, A., Weingartner, E., Wilhelm, R. and Wang, Y. Q.: Characterization and intercomparison of aerosol absorption photometers: Result of two intercomparison workshops, Atmospheric Measurement Techniques, 4(2), 245–268, doi:10.5194/amt-4-245-2011, 2011.

Müller, T., Nowak, A., Wiedensohler, A., Sheridan, P., Laborde, M., Covert, D. S., Marinoni, A., Imre, K., Henzing, B., Roger, J. C., Dos Santos, S. M., Wilhelm, R., Wang, Y. Q. and De Leeuw, G.: Angular illumination and truncation of three different integrating nephelometers: Implications for empirical, size-based corrections, Aerosol Science and Technology, 43(6), 581–586, doi:10.1080/02786820902798484, 2009.

Park, K., Kittelson, D. B. and McMurry, P. H.: Structural properties of diesel exhaust particles measured by Transmission Electron Microscopy (TEM): Relationships to particle mass and mobility, Aerosol Science and Technology, 38(9), 881–889, doi:10.1080/027868290505189, 2004.

Park, S. H., Rogak, S. N., Bushe, W. K., Wen, J. Z. and Thomson, M. J.: An aerosol model to predict size and structure of soot particles, Combustion Theory and Modelling, 9(3), 499–513, doi:10.1080/13647830500195005, 2005.

Petzold, A., Gysel, M., Vancassel, X., Hitzenberger, R., Puxbaum, H., Vrochticky, S., Weingartner, E., Baltensperger, U. and Mirabel, P.: On the effects of organic matter and sulphur-containing compounds on the CCN activation of combustion particles, Atmospheric Chemistry and Physics, 5(12), 3187–3203, doi:10.5194/acp-5-3187-2005, 2005.

Pöschl, U.: Atmospheric aerosols: Composition, transformation, climate and health effects, Angewandte Chemie - International Edition, 44(46), 7520–7540, doi:10.1002/anie.200501122, 2005.

Purcell, E. M. and Pennypacker, C. R.: Scattering and Absorption of Light by Nonspherical Dielectric Grains, The Astrophysical Journal, 186, 705, doi:10.1086/152538, 1973.

Rissler, J., Messing, M. E., Malik, A. I., Nilsson, P. T., Nordin, E. Z., Bohgard, M., Sanati, M. and Pagels, J. H.: Effective density characterization of soot agglomerates from various sources and comparison to aggregation theory, Aerosol Science and Technology, 47(7), 792–805, doi:10.1080/02786826.2013.791381, 2013.

Rissler, J., Swietlicki, E., Bengtsson, A., Boman, C., Pagels, J., Sandström, T., Blomberg, A. and Löndahl, J.: Experimental determination of deposition of diesel exhaust particles in the human respiratory tract, Journal of Aerosol Science, 48, 18–33, doi:10.1016/j.jaerosci.2012.01.005, 2012.

Romshoo, B., Müller, T., Pfeifer, S., Saturno, J., Nowak, A., Ciupek, K., Quincey, P. and Wiedensohler, A.: Optical properties of coated black carbon aggregates: Numerical simulations, radiative forcing estimates, and size-resolved parameterization scheme, Atmospheric Chemistry and Physics, 21(17), 12989–13010, doi:10.5194/acp-21-12989-2021, 2021.

Schkolnik, G., Chand, D., Hoffer, A., Andreae, M. O., Erlick, C., Swietlicki, E. and Rudich, Y.: Constraining the density and complex refractive index of elemental and organic carbon in biomass burning aerosol using optical and chemical measurements, Atmospheric Environment, 41(5), 1107–1118, doi:10.1016/j.atmosenv.2006.09.035, 2007.

https://doi.org/10.5194/egusphere-2022-573
Preprint. Discussion started: 2 August 2022

Schmidt-Ott, A.: In situ measurement of the fractal dimensionality of ultrafine aerosol particles, Applied Physics Letters, 52(12), 954–956, doi:10.1063/1.99239, 1988.

Smith, A. J. A. and Grainger, R. G.: Simplifying the calculation of light scattering properties for black carbon fractal aggregates, Atmospheric Chemistry and Physics, 14(15), 7825–7836, doi:10.5194/acp-14-7825-2014, 2014.

Sorensen, C. M.: The mobility of fractal aggregates: A review, Aerosol Science and Technology, 45(7), 765–779, doi:10.1080/02786826.2011.560909, 2011.

Sumlin BJ, Heinson WR, Chakrabarty RK. Retrieving the Aerosol Complex Refractive Index using PyMieScatt: A Mie Computational Package with Visualization Capabilities, J. Quant. Spectros. Rad. Trans., 205, 127-134. DOI: 10.1016/j.jqsrt.2017.10.012, 2018.

Wentzel, M., Gorzawski, H., Naumann, K. H., Saathoff, H. and Weinbruch, S.: Transmission electron microscopical and aerosol dynamical characterization of soot aerosols, Journal of Aerosol Science, 34(10), 1347–1370, doi:10.1016/S0021-8502(03)00360-4, 2003.

Wiedensohler, A., Andrade, M., Weinhold, K., Müller, T., Birmili, W., Velarde, F., Moreno, I., Forno, R., Sanchez, M. F., Laj, P., Ginot, P., Whiteman, D. N., Krejci, R., Sellegri, K. and Reichler, T.: Black carbon emission and transport mechanisms to the free troposphere at the La Paz/El Alto (Bolivia) metropolitan area based on the Day of Census (2012), Atmospheric Environment, 194, 158–169, doi:10.1016/j.atmosenv.2018.09.032, 2018.

Wiedensohler, A., A. Wiesner, K. Weinhold, W. Birmili, M. Hermann, M. Merkel, T. Müller, S. Pfeifer, A. Schmidt, T. Tuch, F. Velarde, P. Quincey, S. Seeger and A. Nowak (2018). Mobility Particle Size Spectrometers: Calibration Procedures and Measurement Uncertainties. Aerosol Science & Technology 52(2), 146–164.

Wiedensohler, A., Birmili, W., Nowak, A., Sonntag, A., Weinhold, K., Merkel, M., Wehner, B., Tuch, T., Pfeifer, S., Fiebig, M., Fjäraa, A. M., Asmi, E., Sellegri, K., Depuy, R., Venzac, H., Villani, P., Laj, P., Aalto, P., Ogren, J. A., Swietlicki, E., Williams, P., Roldin, P., Quincey, P., Hüglin, C., Fierz-Schmidhauser, R., Gysel, M., Weingartner, E., Riccobono, F., Santos, S., Grüning, C., Faloon, K., Beddows, D., Harrison, R., Monahan, C., Jennings, S. G., O"Dowd, C. D., Marinoni, A., Horn, H. G., Keck, L., Jiang, J., Scheckman, J., McMurry, P. H., Deng, Z., Zhao, C. S., Moerman, M., Henzing, B., De Leeuw, G., Löschau, G. and Bastian, S.: Mobility particle size spectrometers: Harmonization of technical standards and data structure to facilitate high quality long-term observations of atmospheric particle number size distributions, Atmospheric Measurement Techniques, 5(3), 657–685, doi:10.5194/amt-5-657-2012, 2012.

Witten, T. A. and Sander, L. M.: Diffusion-limited aggregation, Physical Review B, 27(9), 5686–5697, doi:10.1103/PhysRevB.27.5686, 1983.

Wozniak, M., Onofri, F. R. A., Barbosa, S., Yon, J. and Mroczka, J.: Comparison of methods to derive morphological parameters of multi-fractal samples of particle aggregates from TEM images, Journal of Aerosol Science, 47, 12–26, doi:10.1016/j.jaerosci.2011.12.008, 2012.

Wu, Y., Cheng, T., Liu, D., Allan, J. D., Zheng, L. and Chen, H.: Light Absorption Enhancement of Black Carbon Aerosol Constrained by Particle Morphology, Environmental Science and Technology, 52(12), 6912–6919, doi:10.1021/acs.est.8b00636, 2018.

Zhang, F., Guo, H., Chen, Y., Matthias, V., Zhang, Y., Yang, X. and Chen, J.: Size-segregated characteristics of organic carbon (OC), elemental carbon (EC) and organic matter in particulate matter (PM) emitted from different types of ships in China, Atmospheric Chemistry and Physics, 20(3), 1549–1564, doi:10.5194/acp-20-1549-2020, 2020.